TRIBHUVAN UNIVERSITY

INSTITUTE OF ENGINEERING

PULCHOWK CAMPUS

THESIS NO.: S014/075

Seismic Vulnerability Assessment of Mixed Masonry-RC Residential Buildings

by

Pranav Acharya

A THESIS

SUBMITTED TO THE DEPARTMENT OF CIVIL ENGINEERING

IN PARTIAL FULFILLMENT OF THE REQUIREMENT FOR THE DEGREE OF

MASTER OF SCIENCE IN

STRUCTURAL ENGINEERING

DEPARTMENT OF CIVIL ENGINEERING

LALITPUR, NEPAL

SEPTEMBER, 2021

COPYRIGHT

TRIBHUVAN UNIVERSITY
INSTITUTE OF ENGINEERING
PULCHOWK CAMPUS
DEPARTMENT OF CIVIL ENGINEERING

The undersigned certify that they have read, and recommended to Institute of Engineering for acceptance, a thesis report entitled **"Seismic Vulnerability Assessment of Mixed Masonry-RC Residential Buildings"** submitted by Mr. Pranav Acharya (075MSStE014) in partial fulfillment of the requirements for the degree of Master of Science in Structural Engineering.

Supervisor, Dr. Gokarna Bahadur Motra Professor, Department of Civil Engineering IOE, TU	External Examiner, Er. Ganga Bahadur Basnet Senior Divisional Engineer, DoLIDAR
Co-supervisor, Er. Arun Poudel Assistant Professor Department of Civil Engineering IOE, TU	Coordinator, Dr. Kamal Bahadur Thapa M.Sc. Structural Engineering Department of Civil Engineering IOE, TU

Date: September, 2021

ABSTRACT

The practice of unreinforced masonry has been around since ages. In seismically active zones like Nepal, it is utmost for the structures to be designed by following proper seismic design criteria. However, the majority of older unreinforced buildings in Nepal are non-engineered or semi-engineered constructions with inadequate seismic detailing. A detailed visual assessment of the Panauti municipality area, led to the identification of a unique building typology. The term “mixed Masonry-RC” represents the typology with one or two centrally located reinforced concrete columns supporting concrete slabs and beams spanning along the grid of columns which altogether rest over peripheral load bearing unreinforced brick masonry in cement mortar. A total of five building models were taken which belonged to this typology. The buildings were modelled in SAP2000 and pushover analysis was performed. This was followed by generation of fragility curves under different Peak Ground Accelerations (PGAs) of response spectra in NBC 105:2020. The fragility curves thus obtained were used to understand the vulnerability of the structure to considered earthquakes. This study can be further extended for the seismic assessment of similar typology buildings and for appropriate recommendation of strengthening measures.

ACKNOWLEDGEMENT

I would like to take this opportunity to express my profound gratitude to my Supervisor Prof. Dr. Gokarna Bahadur Motra and Co-Supervisor Asst. Professor Er. Arun Paudel, whose untiring help, guidance and practical suggestions inspired me throughout the research and thus accomplish this research work.

I am deeply indebted to Assoc. Prof. Dr. Kshitij Charana Shrestha for his guidance and support from the very beginning and throughout the thesis work. Without his constant encouragement and input, this thesis work could not have taken shape.

I am grateful to the Department of Civil Engineering, Pulchowk Campus, Institute of Engineering for giving me the opportunity to execute this research project as a part of the MSc. Dissertation.

I am extremely thankful to the team at CRS Nepal, ASF Nepal, CRAterre and the authorities at Panauti Municipality for providing the necessary platform to carry out this thesis work.

I am also thankful to my colleagues for Masters in Structural Engineering 2075 batch for their support and encouragement during the work.

I am indebted to my family for their endless love and moral support, and encouragement during my entire study period.

Pranav Acharya

075/MSStE/014

September, 2021

TABLE OF CONTENTS

LIST OF TABLES

LIST OF FIGURES

1. INTRODUCTION

1.1. Background

The load bearing action of unreinforced masonry (URM) is owed to the assembled masonry units, which may be bricks, stone, or concrete blocks; with specified bond patterns; bound together with mortar. Unreinforced masonry (URM) buildings are known to have been constructed for a long time on a worldwide scale.

In the Nepalese context, the unreinforced masonry structures have been a choice for long mostly because of the availability of locally manufactured brick units which would then be bonded together in mortars like lime and cement. Historical masonry buildings were constructed by using more conventional mortars like lime, lime-surkhi mix, etc.

Unreinforced masonry has been the face of an affordable and cost-effective housing construction technique in the context of Nepal. High vulnerability to earthquakes creeps in inevitably with this form of construction owing to the multitude of critical points within such structures and thus these structures are found to be more vulnerable to damage during earthquake shaking.

Upon observing the nature of structures which failed to resist the ground shaking, it would lead us to confirm that the masonry structures which have been built in poor accordance with the building codes, poor construction practice, poor construction materials, inadequate joint connections, and houses with stories added up to suffice the expanding family in core urban areas faced major damages during earthquakes. Not only the residential but the historical masonry structures also faced huge damages in the 2015 earthquake. Poorly planned and unmanaged settlement expansions and construction practices further bolstered practices involving a lack of engineering design and detailing in Nepal. The disastrous Gorkha earthquake of 2015 and its effects on the then constructed masonry structures reconfirmed the susceptibility of such structures to shaking hazards. Similar is the case with poorly constructed RCC structures too.

1.2. Need for study

Nepal is located in one of the world's most seismically active locations, in the Himalayan range, on the boundary between the Eurasian and Indian plates, where

Nepal has long been subjected to several powerful earthquakes. Throughout its history, Nepal has experienced several strong earthquakes and six great damaging earthquakes in the years 1255, 1408, 1505, 1833, 1934, and 2015 with magnitudes equal to or greater than 7.6 (Thapa et al., 2017). The 2015 Gorkha earthquake caused lots of destruction in various forms of structures built in Nepal. Most of the damages were seen in older masonry structures in core residential areas of the districts of Kathmandu, Bhaktapur and Lalitpur.

According to the damage data collected by the Ministry of Home Affairs, district level distribution of building types defined in the 2011 National Census, and differential fragility of buildings assessed by the National Society of Earthquake Technology (NSET), 18,214 fully damaged cement mortared masonry, while 474,025 low strength masonry, 65,859 partially damaged cement mortared masonry and 173,867 partially damaged masonry.

The majority of Nepalese construction uses unreinforced masonry, which consists of solid brick, concrete block, or stone, and is mortared with either cement or mud, with styles differing according to the region where the construction is carried out and the building age (Build Change reports, 2015).

The seismic vulnerability of URM buildings leads to the destruction during earthquakes in a large scale. Fifty-eight percent of all housing construction are low strength masonry stone or brick masonry with mud mortar, which lack seismic-resilient features. These buildings are intrinsically weak and brittle, and thus suffered widespread damage throughout the 31 districts that experienced intense ground shaking; according to National Planning Commission Post disaster need assessment, 2015.

It is thus important to take control on the factors that would tend to help minimize the earthquake damage from earthquakes in future. (The Code of Practice for Structural Use of Unreinforced Masonry, IS:1905-1987) mentions that the structural sufficiency of masonry walls is determined by a number of factors, including the quality and strength of masonry units and mortars, workmanship, unsupported height of walls, load eccentricity in walls, the location and size of openings in walls, and the combination of various external loads to which walls are exposed.

The detailed visual assessment of the Panauti municipality area based on the contextual assessment framework proposed by CRS-IOE-ASF Nepal-CRAterre led to the identification of a unique building typology in the Panauti area. The identified masonry-RC typology has one or two centrally located RCC columns that support concrete slabs and beams spanning along the grid of columns which altogether rested over load bearing brick masonry in cement mortar over the periphery of the building. This form of construction practice prevailing in this area helps to infer that people believe in taking some strengthening measures through the use of RCC columns without which it would simply be load-bearing masonry wall system. However, this form of construction can be critical in the face of strong ground shakings, chiefly because of lack of appropriate joint connections, lack of bands, inadequate thickness and poor load transfer. These kinds of shortcomings in masonry buildings make them vulnerable to earthquakes. It is thus important to assess the seismic behavior of these structures.

In this thesis, the analysis of five such building models with the typology as explained earlier is done. The three building models exist in real while the remaining two are fictious, modeled according to the common structural configurations as observed in the Panauti area. The three models differ in the storey height, the plan dimensions, area of openings, shape of columns and the layout of beams in plan. Firstly, static analysis of the masonry building is done using 3D simplified macro modelling approach. Then, nonlinear links have been introduced according to the predefined conventional crack patterns as well as observed cracks in the walls. Then, pushover analysis is performed to study its nonlinear behavior in in-plane direction. The performance point is then calculated from Capacity Spectrum Method and fragility curves are generated to check seismic vulnerability levels.

1.3. Objectives

The main objective of the work is:

1. To assess the vulnerability of the selected typology residential buildings though fragility curves

1.4. Scope of the Work

1. The proposed study has direct implication towards strengthening of vulnerable residential buildings in Panauti municipality.
2. In general, this study highlights the vulnerabilities of the existing typical URM residential buildings through a more detailed nonlinear push-over analysis and fragility curves.

1.5. Limitations

1. A comprehensive pool of different typologies could provide a better picture of the state of vulnerability; representing the whole building population, which is beyond the scope of this thesis.
2. Nonlinearities are concentrated at frame hinges, and NL links whose locations are defined by user based on the predefined conventional cracking patterns and stress concentrations. A more detailed micro-modeling approach or damage models could provide better representation of the failure patterns and capacity curves, a limitation for FE modeling using SAP2000.
3. Fragility curve generation is based on capacity spectrum method (CSM) from nonlinear push-over curves. Non-linear time history analysis could give more comprehensive results but would require input of more detailed dynamic characteristics of the structure, which is not available to the author at present.

1.6. Organization of the Study

The entire thesis is divided into following five chapters.

Chapter 1 is an introduction to the present study which includes background, need for study, objective, scope, and limitation of the study.

Chapter 2 includes the literature review about the properties of unreinforced masonry, previous damage data related to the damage of unreinforced masonry structures due to past earthquakes, failure modes in case of URM, modelling and analysis techniques of the URM, non-linear static(pushover) analysis and some relevant literatures in the context of Nepal.

Chapter 3 presents methodology followed in the thesis work with techniques for the nonlinear analysis and retrofitting solutions. It includes the selection of the prototype, the visual assessment details, relevant drawings, model validation, the modelling approach, material and section properties, nonlinear link properties; their definitions, arrangement in the model

Chapter 4 presents the analytical results which are obtained from modeling and discussion of the results thus obtained

Chapter 5 presents conclusive statements from the research work and recommendations for further study

2. LITERATURE REVIEW

2.1. Background

This chapter provides analytical review on relevant past literatures carried out during the study. The properties of unreinforced masonry, previous damage data related to the damage of unreinforced masonry structures due to past earthquakes, failure modes in case of URM, modelling and analysis techniques of the URM, non-linear static(pushover) analysis and some relevant literatures in the context of Nepal have been presented.

2.2. Unreinforced Brick Masonry

Unreinforced masonry is commonly used in the form of low-rise residential and office buildings in which the whole area of the floor is divided into a large number of spaces which extend from the foundation up to the roof level (Hendry et al. 1997). This approach supports the flexibility with which the load bearing walls can be placed and arranged, which are the backbones of the force-resisting members in the URM structural system. It is mandatory that more economical and more environment-friendly construction typologies are constructed. For developed as well as developing countries, the URM form of construction can thus play an important role (Marques et al., 2011).

Masonry exhibits a nonlinear nature in case of compression, and only a negligible tensile strength (Garbin et al., 2007). During the course of time, specific features have been invented which have improved the seismic behavior of masonry buildings. The strengthening of comers and wall intersections zones, tying of the walls, etc. are some of these specific features. However, the construction of masonry still represents the most vulnerable part of existing building stock (Tomazevic, 2006).

All URM walls have a common materials strength characteristic. These materials have a tensile modulus of rupture much less than their compressive strength. The tensile cracks commonly occur on a mortar unit interface or within the mortar joint. Inter-story displacement resulting from earthquake induced internal forces may cause cracking due to combined axial, flexure and shear stresses (ABK, 1984).

2.3. Damage Data

Around 700,000 buildings were damaged by the 2015 Gorkha Earthquake which was of 7.8 Magnitude. About 58% of the buildings are mud-based masonry, 21% are cement-based masonry (stone with cement-sand mortar or brick with cement-sand mortar) and about 15% are reinforced concrete with masonry infill while the rest covering only 6% of the typologies amongst the building typologies spread across 31 districts which had been severely affected by the 2015 Gorkha earthquake (Tiwari et al. 2020).

According to the National Reconstruction Authority (NRA), of 1,047,261 damaged houses surveyed, 78.4 percent were of low strength masonry, 7.87 percent cement-mortared masonry and only 3.57 percent were reinforced concrete houses.

According to International Nepal Fellowship, one of the recent aftershocks of the Gorkha earthquake, which was reported by the National Earthquake Monitoring and Research Centre was of 5.4 and 5.8 Richter in magnitude. This aftershock damaged 140 houses in the Lamjung district including a big portion of the masonry houses.

Because Nepal is in a seismically active region where earthquakes occur often, structures in Nepal must be designed and built to withstand earthquakes. Nepalese structures, on the other hand, are largely non-engineered or semi-engineered and lack seismic resistant details. In the past, earthquakes in Nepal, notably the Kathmandu valley, have resulted in major structural damage and human deaths. Previous earthquakes have wreaked havoc on Nepalese infrastructure, demonstrating their vulnerability (Shrestha et al. 2016).

2.4. In-plane and out-of-plane actions of URM

In-plane actions of URM walls are divided into five categories. Rocking and bed-joint sliding, which involves stair-step cracking through head and bed joints, are two deformation-controlled in-plane movements of URM walls. Toe crushing, diagonal tension that produces cracking through the masonry units, and vertical compression are all force-controlled in-plane actions of URM walls (ASCE 41-13).

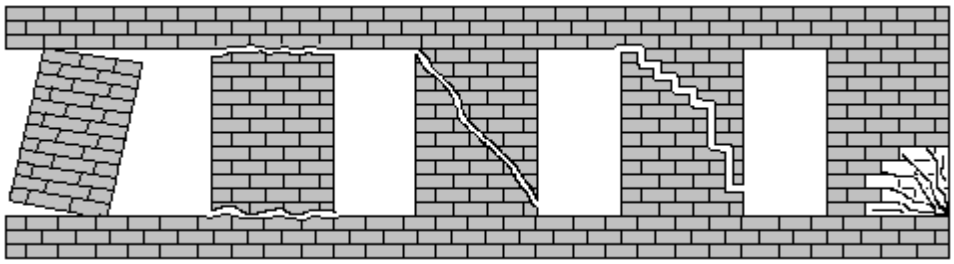

Figure 2.1 Rocking, Sliding, Diagonal Tension and Toe Crushing in Masonry wall (Tianyi Yi, 2004)

Rocking or sliding governs the response of URM piers with low levels of vertical axial stress. Large displacement capacities have been observed in these actions.

2.4.1. In-plane actions of URM

A load-bearing masonry structure is normally constructed as a vertical cantilever for acceptable compressive and shear stresses without tension. At floor-to-wall connections, no moment transmission is allowed, and lateral forces are supposed to be resisted by diaphragm action of floor/roof slabs, which operate as horizontal beams and convey lateral forces to cross walls in proportion to their respective moments of inertia. Some of the modes of failure of unreinforced masonry are as shown in fig. 2.2 through fig. 2.5, (D.C. Rai, Structural use of unreinforced masonry: Code and Commentary).

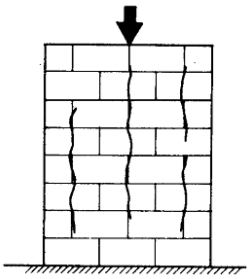

Figure 2.2 Splitting of wall in tension under action of vertical compressive load

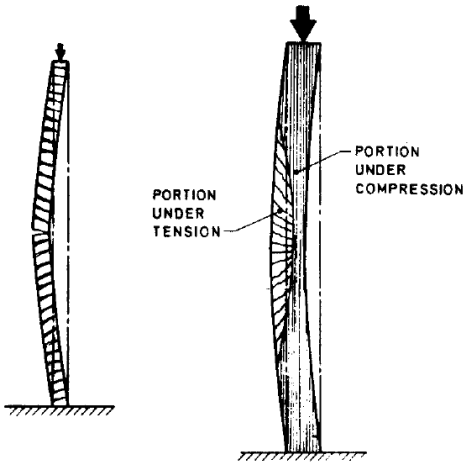

Figure 2.3 Buckling of a wall under vertical compressive load

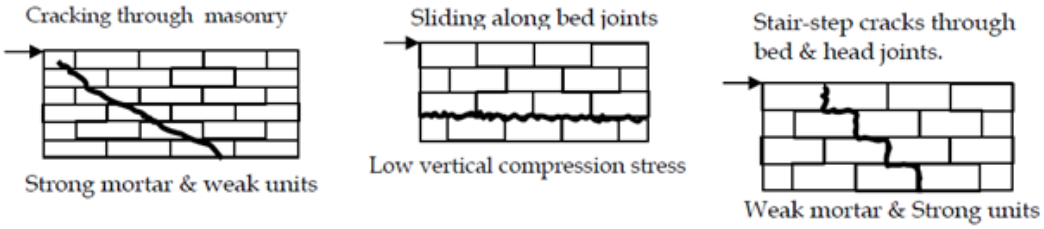

Figure 2.4 Shear failure of a masonry cross wall under lateral loading

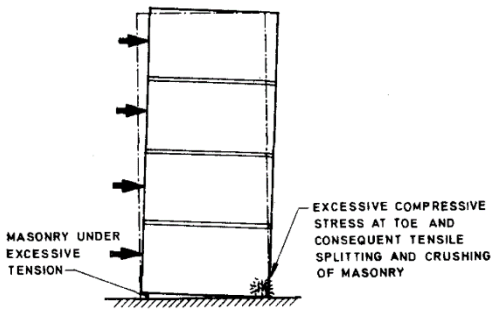

Figure 2.5 Crushing of masonry at toe

Unreinforced masonry (URM) constructions can fail due to structural weakness or overloading, dynamic vibrations, settlements, and in-plane and out-of-plane deformations (Tomazevic, 2006). Non-wall component damage frequently develops before in-plane wall damage becomes noticeable. The most of modes are related to in-

plane damage, but out-of-plane damage also could occur along with in-plane damage (FEMA 306). The dominant failure mechanism is the mechanism that results in lower lateral resistance and it corresponds to the maximum lateral load.

Deformation-controlled actions are those that are expected to result in a ductile behavior in the member without a significant loss of strength. Force-controlled actions are expected to exhibit brittle behavior. In earthquake resistant design techniques, force-controlled members are not allowed to reach the yield stress. Lower bound strengths and anticipated strengths of materials are used in seismic evaluation recommendations such as FEMA 356 and ASCE 41-06 so as to determine the capacity of force-controlled and deformation-controlled actions, respectively (Ghiassi et al. 2012).

2.4.1.1. Bed joint sliding failure

The bed-joint sliding failure is considered as a deformation-controlled action in FEMA 356. The masonry shear strength against this failure mode can be calculated with the aim of friction theories and is proposed by FEMA 356 as follows:

$$V_{bjs} = v_{me} V_{bjs} A_n \tag{2.1}$$

where,

V_{bjs} is the bed-joint sliding capacity of the masonry

A_n is the area of mortar,

v_{me} is the expected masonry shear strength.

2.4.1.2. Rocking

When the wall shear strength is high, the wall is slender, and the compressive stresses are low, rocking is common. It's frequently accompanied by a considerable deformation capacity, which is limited by toe compression failure or wall instability. When rocking behavior repeats itself in multiple cycles, toe crushing may occur. For rocking and toe crushing, equations are recommended in FEMA 356 and ASCE 41-06 to calculate the shear strength of the URM.

$$V_r = 0.9\alpha \, P_E \frac{L}{h_{eff}} \tag{2.2}$$

$$V_{tc} = \alpha\, P_L \frac{L}{h_{eff}} (1 - \frac{f_a}{0.7f'_m}) \quad (2.3)$$

where,

Vr is the wall rocking capacity,

Vtc is the wall toe crushing capacity,

PL is the lower bound axial compressive force due to gravity loads,

fa is the axial compressive stress due to gravity loads, and

f 'm is the lower bound compressive strength of masonry.

α a factor equal to 0.5 for cantilever walls and 1.0 for fixed-fixed walls,

PE is the expected axial compressive force due to gravity loads,

heff is the height to resultant force

2.4.1.3. Diagonal tension

A diagonal crack spreads across the wall in diagonal tension behavior. Strong mortar, weak units, and high compressive stresses are common causes of this behavior in walls. Small nonlinear deformations are expected in this scenario. The majority of the time, cracking develops unexpectedly, and the wall strength quickly deteriorates. FEMA 356 proposes the following equation for estimating the diagonal tension capacity of the wall:

$$V_{dt} = A_n f_{dt} \frac{L}{h_{eff}} \sqrt{\frac{f_a}{f_{dt}} + 1} \quad (2.4)$$

where,

Vdt is the diagonal tension capacity of the wall

f dt is the lower bound diagonal tension strength of the masonry

2.4.2. Out-of-plane actions of URM

In analytical models that analyze the features of the global structural system in the orthogonal direction, the out-of-plane stiffness of walls is ignored. When effective wall-to-diaphragm connections are present, out-of-plane stability of URM walls is evaluated for out-of-plane inertial forces by considering components to span vertically

between diaphragm levels, or horizontally between intersecting walls, columns, or pilasters, or to span with two-way action. Some of the out of plane failure mechanisms (D'Ayala and Speranza, 2003) can be seen in fig. 2.6.

Jaroslav Vaculik (2012) Although out-of-plane activity isn't usually considered part of a building's seismic load path, the walls nevertheless need to be strong enough to prevent out-of-plane collapse. Local failure can pose a significant risk to life safety, and failure of load-bearing walls can cause partial or complete collapse of the overall structure by compromising gravity or lateral in-plane load resistance paths. In post-earthquake study, out-of-plane wall collapse has been identified as one of the most common modes of failure in URM construction.

Paulay T., Priestley M.J.N (1992) The response of unreinforced masonry to out-of-plane seismic excitation is one of the most difficult and poorly understood parts of seismic analysis. The in-plane and out-of-plane responses in the walls are induced by the multiaxial nature of ground shaking caused by seismic forces. The inertia mass of the walls reacting to the floor-level excitation will generate the out-of-plane response. The input motion that the face-loaded wall "sees" will be considerably different from the earthquake ground motion, with strong harmonic components that represent the structure's inherent frequencies.

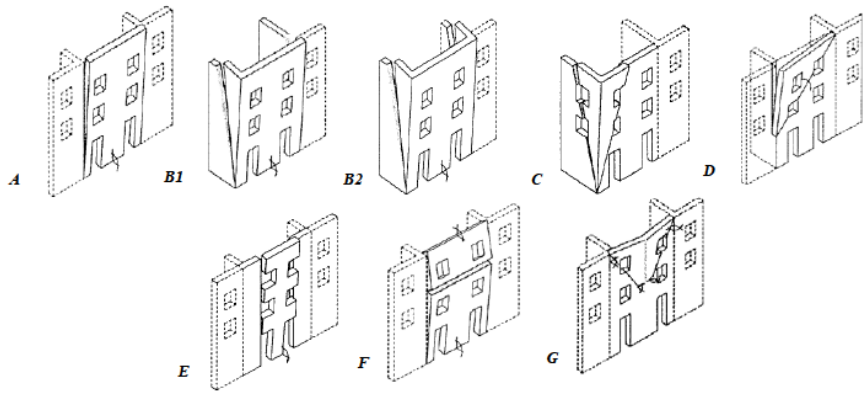

Figure 2.6 Out of plane failure mechanisms (after D'Ayala and Speranza (2003)

2.6. Analytical Modelling Techniques in Masonry

Ivo Caliò (2014) A thorough finite element technique can provide a wealth of information about the nonlinear behavior of the component materials, as well as their interaction and local and global collapse causes. Even yet, both the modeling and the data interpretation steps are exceedingly time demanding.

Masonry is a material with distinct directional properties due to mortar joints that act as planes of weakness; the numerical representation approach can focus on the micro-modeling of individual components and mortar, or the macro-modeling of masonry as a composite, and depending on the level of accuracy and simplicity desired, the following modeling strategies are used (Lourenço, 1996; Campbell, 2017).

1. Detailed micro-modeling - The bricks and mortar are modeled as continuous elements with specific failure criteria in this form of modeling. Special elements that depict the discontinuities are used to model the interface between bricks and mortar. The geometry of the wall is completely replicated in this case. Because of the level of detail in this model, it is considered to be capable of representing most masonry failure mechanisms.

2. Simplified micro-modeling - The bricks remain the same as they were in the "detailed micro model," but the mortar joints and interface parts are re-defined as distinct elements to depict a contact region. The overall geometry is preserved, but the individual parts that indicate joints and interfaces are unable to explain the Poisson's effect of mortar over bricks. Some forms of failure mechanisms cannot be duplicated in this type of model.

3. Macro-modeling - The masonry panel (or a portion of it) is considered a homogeneous element in this scenario. This type of model should be able to recreate the basic structural behavior of a masonry panel due to its properties, but it will not be able to simulate all forms of failure processes.

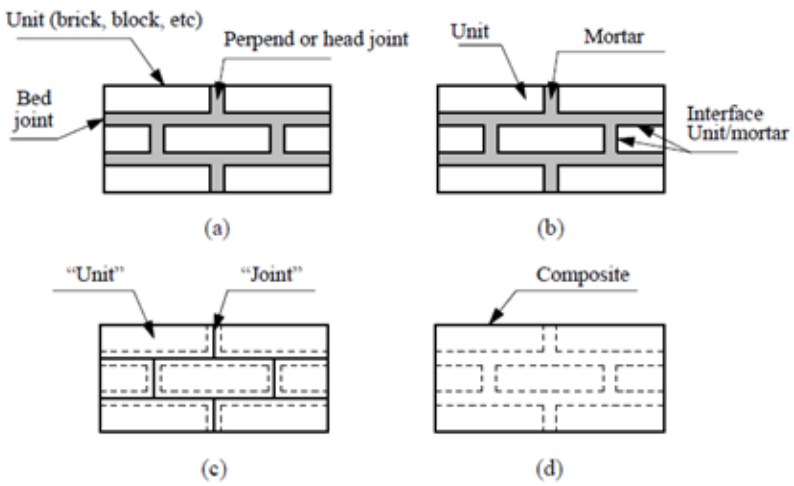

Figure 2.7 Modelling strategies for masonry structures: (a) Masonry sample; (b) detailed micro-modeling; (c) simplified micro- modeling; (d) macro-modeling

2.7. Link Elements

Link is a two joint connecting element and according to the types of properties assigned to that element and the type of analysis being performed, each link element may exhibit up to three different types of behavior: linear, nonlinear, and frequency-dependent, and each link element may exhibit up to six degrees of freedom (axial, shear, torsion, and bending). The nonlinear force-deformation relationships are employed in nonlinear analysis at all degrees of freedom for which nonlinear features were given.

Tomazevic (2006) states that lateral load-displacement relations, failure mode, and crack patterns can be predicted relatively well using a finite element technique (FEM), in which masonry blocks and mortar joints are treated as discrete or continuous elements with links between them.

The NL link element is a special link element that permits user-defined force and deformation relations to be used to describe material nonlinearity (Sanchez Bravo, 2012). To represent both axial and shear behavior, the force-deformation relationships assigned to nonlinear links are defined as Multilinear Plastic link elements, where the axial deformation is defined by the longitudinal direction of the link elements and the shear behavior is defined by the in-plane transverse direction (Sanchez Bravo, 2012). The tributary area of wall elements represented by each of these nonlinear links

influences the force vs deformation data. The nonlinear links' axial response characteristics directly impact the wall's flexural behavior.

For simulating the axial response in compression by the nonlinear links, both the contributions from masonry and reinforcement elements is taken into account (for reinforced masonry). But in tension, the contribution of masonry is almost neglected. Thus, in URM walls, the tension part is represented by a horizontal line with zero force. Peak forces are obtained after assigning 0.8 f'm to the masonry in compression and fy to the reinforcing steel in tension and compression. The stiffness in tension and compression are both taken as zero after yielding.

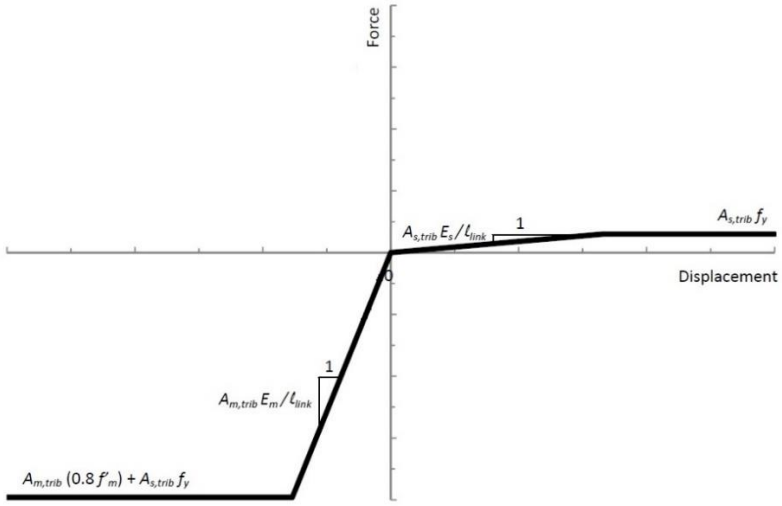

Figure 2.8 Non - Linear Link Definition for Reinforced Masonry Wall, Axial Direction

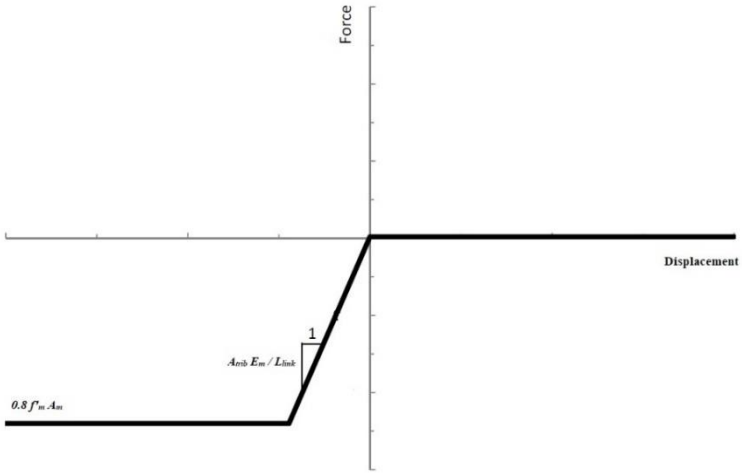

Figure 2.9 Non - Linear Link Definition for URM Wall, Axial Direction

The force-deformation relationships assigned to the nonlinear links for modelling the reaction in shear are characterized as bilinear and symmetrical. The first line represents the stiffness of the wall segment based on gross-section parameters, whereas the second line represents the nominal shear strength of the wall segment and is horizontal. The shear response links are defined in such a way that the shear carried by the link generates a secondary moment only at one end. A flexurally-rigid line element is introduced to fully embrace the wall cross section to properly account for the effects of the secondary moment.

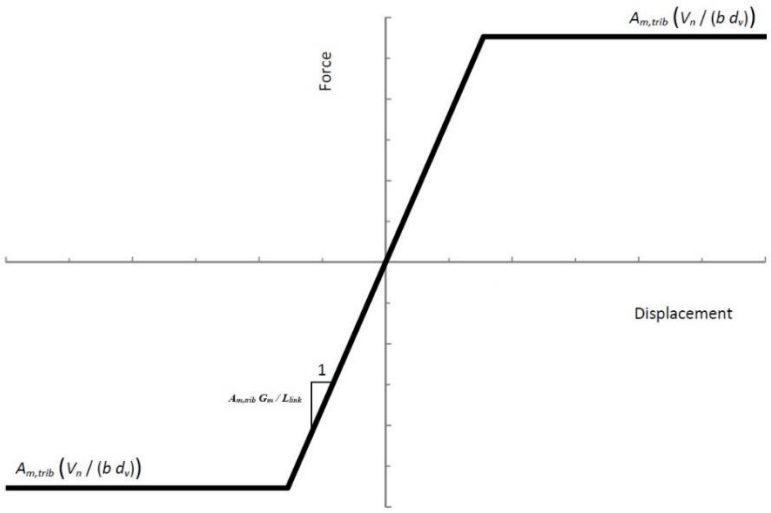

Figure 2.10 Non - Linear Link Definition, Shear Direction

2.8. Non-Linear Static Analysis: Pushover Analysis

The nonlinear static procedures estimate the maximum global displacement of a structure to shaking at its base; FEMA 306. The NSP is mainly suitable for buildings without significant higher-mode response (FEMA 273). The building model integrating nonlinear load-deformation features is subjected to monotonically increasing lateral loads, reflecting inertial forces in an earthquake, up to a predefined value or state in nonlinear static analysis. According to Displacement Coefficient Method, as per FEMA 356, a target displacement is determined to represent the greatest displacement that is predicted to occur during the design earthquake.

The Capacity Spectrum method is defined by ATC 40, in which a load is incremented and checked at each stage until the "Performance Point" is attained. In proportion to the distribution of inertia forces in the plane of each diaphragm level, lateral loads are

applied to the model. The control node is placed in the center of mass on a building's roof. For control node displacements ranging from zero to 150 percent of the goal displacement, a relationship between base shear force and lateral displacement of the control node should be established (FEMA 356).

By applying loads until the weak spot in the structure is found, a pushover analysis simulates the phenomena in which particular components of structures yield or fail, and the dynamic forces are redistributed to other components. The structure is "pushed" once again until the second weak link is found, and this procedure is repeated until a yield pattern for the entire structure under seismic load is established (Khan, 2013).

In the context of seismic assessment, the role of non-linear equivalent static analysis is being more and more recognized as a useful tool for the correct evaluation of the seismic response of structures in terms of overall strength and deformation and for a correct evaluation of the possible failure mechanisms (Magenes, 1998).

Penelis Gr. G. (2004) established an effective approach for pushover analysis of URM structures that also allows for the prediction of the failure mechanism by observing the development of plastic hinges at various positions throughout the structure. However, it should be noted that these plastic hinges are a computational simulation of the nonlinear behavior of the entire member they correspond to, rather than the actual failure mechanism of URM (due to its brittle nature).

2.9. Capacity Spectrum Method

The capacity spectrum method, developed by Freeman et al. (1975), is a displacement-based design strategy. The capacity spectrum method (CSM) is a nonlinear static analysis method that uses a graphical representation to compare a structure's global force-displacement capacity curve with the earthquake response spectrum (Freeman, 1998). This method compares the seismic activity to the building's load bearing capacity, taking into consideration nonlinear material behavior and post-peak capacity. The building capacity is characterized by a pushover curve, while the seismic activity is represented by a reduced response spectrum due to damping. Both curves are transformed into spectral ordinates for acceleration-displacement responses (ADRS format). The capacity curve as well as the response spectra must be transformed into a spectral acceleration Sa spectral displacement Sd

graph. The global structure will be reduced to an analogous SDF-structure as a result of this transformation. The performance point, which describes the spectral displacement of the building owing to the given earthquake, can be estimated using a trial-and-error process. The point where both curves overlap is known as the "Performance Point," and it corresponds to the highest spectral displacement for the particular site spectrum. The CSM approach is outlined in the ATC 40 (1996), FEMA 273 (1997), and FEMA 274 (1998).

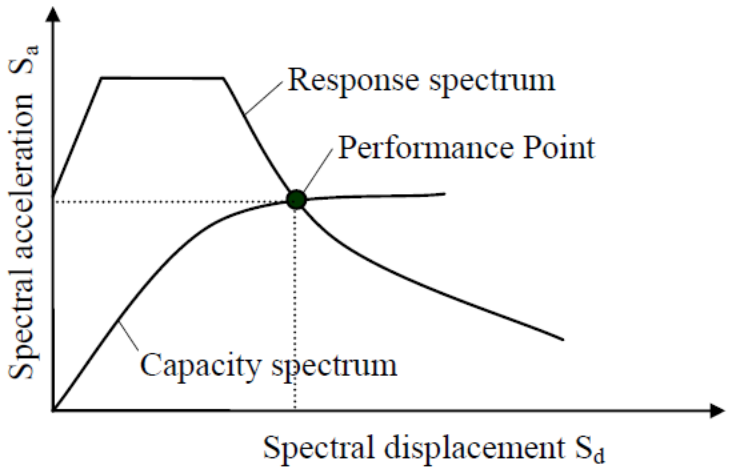

Figure 2.11 Sa-Sd plot of capacity spectrum, response spectrum and performance point

The intersection of an acceleration–displacement spectrum, representing ground motion, and a capacity curve converted to plots of spectral acceleration versus spectral displacement, representing the horizontal displacement of the structure under increasing lateral load, yields the performance point of a building type under a specific ground-shaking scenario.

2.10. Fragility Functions

The probability that a structure will surpass a particular damage state under a certain earthquake shaking level is known as its fragility. The fragility curves aid in determining the structure's seismic risk and the necessary strengthening measures (Tripathi et al. 2018).

The seismic performance level should be objectively quantified through risk assessment of URM structures for reasonable estimation and minimization of potential seismic losses connected with URM structures. Fragility analysis is a useful

method for assessing the risk of structural systems since it allows for the probabilistic estimation of seismic losses and, as a result, decision-making for seismic risk reduction (Park et al., 2009). Seismic fragility analysis of low-rise URM building structures can be employed for fragility analysis without a considerable loss of computation time and with an acceptable level of accuracy in depicting the structures' nonlinear behavior. To produce the fragility curves, the seismic reactions of the URM building subjected to various degrees of earthquake inputs are probabilistically evaluated, taking into account the randomness in various attributes.

Borzi et al. (2008) The fragility curve expresses the probability that the target structure will exceed a specific damage state as a function of earthquake intensity parameters (such as PGA, PGV, Sa etc.). The conditional probability is expressed as:

$$P_{ik} = P[D \geq d_i \mid S = sk\ ] \ldots\ldots. (1)$$

Where P_{ik} is the likelihood that the damage state d_i will be reached or exceeded for a ground motion severity sk, and D and S denote the damage and severity of the input motion, respectively.

Paudel et al. (2021) presented a case study on strengthening of a masonry building inside Pulchowk Campus, which was severely damaged during 2015 Gorkha earthquake. For the analysis of the structure, macro-modelling approach was performed. The analysis was performed in SAP 2000 wherein area elements were defined as non-linear shell element. Four possible options of strengthening were identified, modelled and the obtained results were analyzed. Among the four models, the RC jacketing method modeled using layered links, was found to be the most effective method for retrofitting of the considered building. In this work, RC columns are connected with brick piers through shear-keys as a new approach for retrofitting. Static pushover analyses were done to assess the restored and four retrofitting solutions' capacities. The improvement in masonry performance following the implementation of various retrofitting options was assessed. Retrofitting using RC columns combined with brick piers at the ground level alone was chosen for final execution after a thorough investigation of the acquired results, keeping resource constraints in mind.

Maharjan et al. (2020) assessed recently constructed stone masonry buildings in mud mortar with horizontal reinforced concrete (R.C.) bands. To explore the seismic

performance of stone masonry buildings constructed with horizontal bands, two recently completed stone masonry houses of various geometry were selected, modeled, and assessed. Built with stone and mud mortar, the stone masonry wall was modeled in shell and area. The performance of the selected buildings was assessed using linear time history analysis and other numerical models. Using three earthquake time records, fragility curves were created to determine the likelihood of building failure at various peak acceleration values.

M. Chikanbanjar et al. (2019) used two different modelling strategies to study the nonlinear behavior of unreinforced masonry viz. equivalent frame model and macro element model. Equivalent frame model was implemented in SAP 2000 code, and macro element approach was implemented by 3Muri. Three masonry building made up of brick in cement mortar masonry of same plan configuration but different number of storey were taken into consideration and each of these buildings were analyzed considering flexible floor and rigid floor separately. It was concluded that flexibility of floor has not much effect on the behavior of single storey building but the influence of floor flexibility can be seen for multi-storey building. Unreinforced masonry buildings with rigid floor has high capacity in comparison to flexible floor because rigid floor creates box effect such that all the walls behave as one while in flexible floor walls tend to act individually. SAP2000 is recommended by author; because of simple calculations, fast and ease of implementation. The author also recommended to use appropriate modelling strategies with proper knowledge on the methodology, analysis requirement and the assumptions used in the modelling.

The structural examination and retrofitting of the Shital Niwas building, which was severely damaged during the Gorkha Earthquake, was completed by Sah, Jha, and Motra (2021). The examination revealed issues such as mud mortar masonry's low strength, the heavy weight of the walls and floors, the presence of lengthy unsupported walls under flexible diaphragms, a high ratio of openings, and the lack of earthquake-resistant elements. ETABS was used to create a 3D FEM model with homogenized wall material. At the plinth level, structural masonry walls were represented as thick shell sections with hinge supports. Steel plates and carbon fiber reinforced polymer (CFRP) bands were chosen as a retrofitting approach after extensive analysis and design.

Guragain et al. (2012) This study used the Applied Element Method to construct fragility functions for non-engineered poor earthquake resistant masonry buildings in Nepal. Field tests in real field conditions were used to acquire key parameters for study. The results of the AEM experiment were compared to the results of the shaking table experiment, and they were found to be in good agreement. Buildings of various configurations, material strengths, story counts, and mortar types were numerically simulated, and the likelihood of damage reaching a specified degree of damage state was computed for peak ground acceleration (PGA) ranging from 0.05g to 1.0g. Based on numerical simulation results, fragility functions for low earthquake resistant masonry buildings in various states of damage were presented.

Acharya (2015) evaluated the seismic vulnerability of different selected hospital buildings in Kathmandu valley. The author in his study included six building typologies. A three-dimensional model was developed and analysed in SAP2000 v16. Guidelines of HAZUS-MH-MR3 2003 was adopted for the estimation of displacement capacity during different damage states. The seismic demand was obtained from linear time history analysis. The structural vulnerability of the buildings were expressed in terms of fragility curves (probability of failure vs peak ground acceleration) which defined the probability of the buildings sustaining slight to complete damage in an earthquake based on different levels of ground motion intensity (PGA). The state of vulnerability of such buildings called for rigorous study for proposing and planning suitable retrofitting and rehabilitation programs.

Khadka (2009) studied the seismic performance of unreinforced masonry buildings, wherein a fictious building was analysed to reflect the characterstics of the URM structure. The finite element method was adopted for a number of parametric analyses like the effects of wall thickness, floor rigidity, effect of opening, number of stories so as to determine the response of the fictious building in terms of displacement. The preliminary conclusions from this fictious model were used in analysis of real building, Shital Niwas as a case study. Due to complexity of modelling, only the North wing of the Shital Niwas was modelled ad analysed. The performance of the building was investigated in terms of displacement response and the conclusions of the North wing was generalized for the whole of building configurations. The lesser cross walls connected with longitudinal walls which made larger room sizes led to the inability of the whole building to act as a single unit. The collapse of outer wall of

North wing was due to excessive out of plane deformation. The global behavior of such building was concluded to primarily depend upon loosely connected timber floors and unreinforced masonry walls.

For masonry school building portfolios in Nepal, Giordano et al. (2021) established analytical fragility curves. The authors analyzed the available statistics for Nepalese schools before presenting analytical fragility curves for three URM typologies, namely rubble stone-mud masonry, brick-mud masonry, and brick-cement masonry buildings, which account for more than half of the school building stock. To improve the granularity of the fragility model, assessments were conducted for single-story and multi-story building types. The findings of the analysis were compared to Nepal-specific fragility studies published in the literature. In comparison to the analytical investigation, the new fragilities demonstrate good agreement.

For Nepalese residential buildings, Gautam et al. (2018) established empirical fragility functions. The findings revealed that when subjected to strong to severe earthquakes, most rural residential building stocks (stone masonry) and brick masonry structures in Nepal are highly vulnerable, with the likelihood of extensive damage to collapse (DS-3) being higher than the other damage stages. On the contrary, even in the event of strong to large earthquakes, Nepali residential RC buildings exhibited a minimal level of vulnerability. According to the database used in this study, RC buildings were reported to be damaged in the PGA range of 0.15–0.8 g, whereas brick and stone masonry buildings were found to be damaged in some sites even at 0.075 g PGA.

3. METHODOLOGY

3.1. Introduction

The general methodology adopted for the current study is illustrated in fig. 3.1. The current work is done under project "Nepal Homes and Communities, Baliyo Ghar Baliyo Sahar" with primary focus on a mixed typology- central columns with peripheral load bearing masonry walls. The building typology thus selected represents a major portion of the typology of the buildings present within the Panauti municipality. A detailed visual assessment was done and a detail survey based on the contextual assessment framework proposed by CRS-IOE-ASF Nepal-CRAterre was also performed. The contextual assessment for this building and others representing similar typologies presented. Some of the details of the same can be found in Appendix A of this thesis.

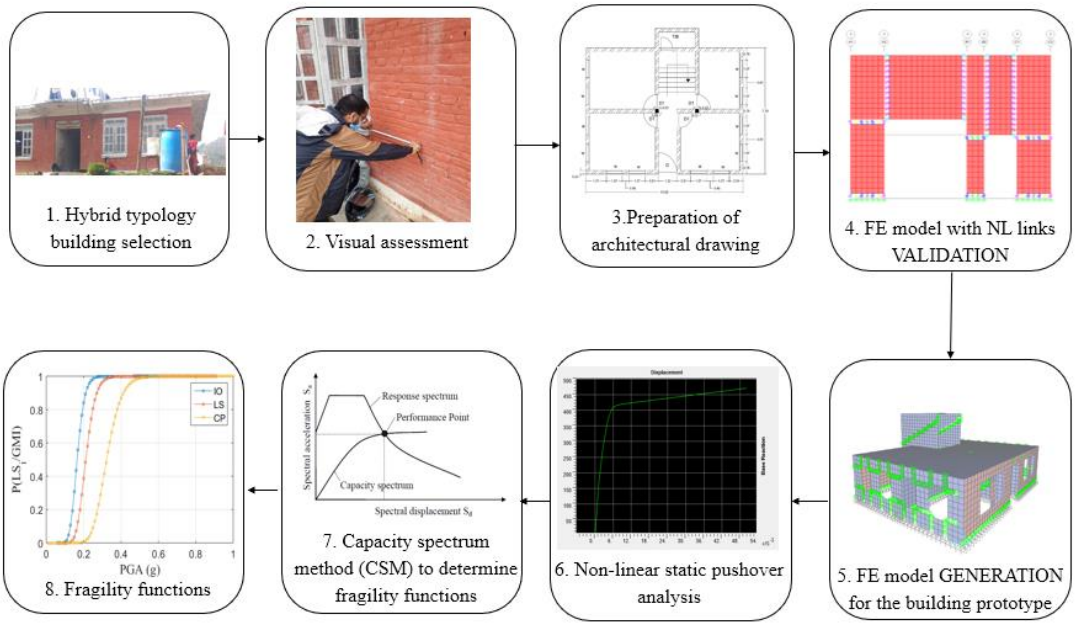

Figure 3.1 General methodology adopted for current study

3.1.1. Selection of Building prototypes

After completion of reconnaissance survey, a building with centrally located RCC columns, beams and slabs with the beam and slab resting over peripheral load bearing brick masonry walls was selected. Similar to the typology considered, two other real building models were also considered. These buildings are located in the Panauti

municipality-04 of Kavrepalanchowk district. The pictures of the selected building prototypes can be found in Appendix-A.

3.1.2. Measurement and visual assessment of the selected building

During the reconnaissance survey, different aspects of the building are visually examined. The important parameters of the building that are required for assessing its vulnerability are measured and recorded. Photographs of the existing condition of the building were also taken for reference during the preparation of the as-built drawing. Damages that have occurred in the building after the earthquake were also identified.

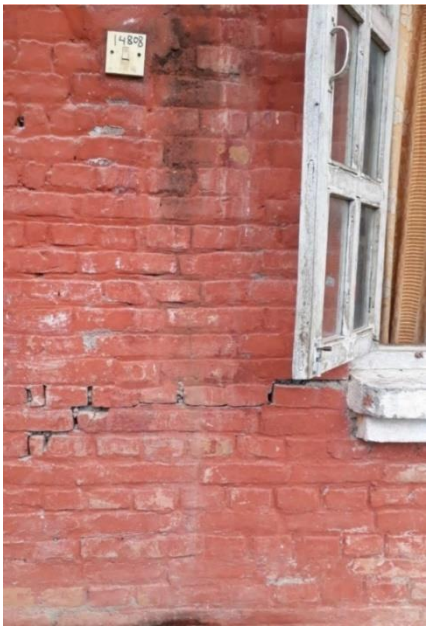

(a) Diagonal Cracks originating from opening

(b) Diagonal Cracks originating from opening

(c) Crack through pier

(d) Diagonal Cracks originating from opening

Figure 3.2 (a), (b), (c), (d): Cracks in masonry

The general building description of the models that have been considered in this thesis is summarized as follows.

Building Model	**Model 1**	**Model 2**	**Model 3**	**Model 4**	**Model 5**
No. of Stories	1	2	4	2	3
Storey height	2.85	2.25	2.4	2.85	2.4
Total height	5.25	5.9	9.6	5.7	9
Floor	RCC, M20	RCC, M20	RCC, M20	RCC, M20	RCC, M20
Wall thickness	230mm	400mm @ GF + 230mm @ FF	230mm	230mm	230mm
Plan dimensions	10.52 x 9m	7.35 x 5.35m	9.4 x 5.8m	11 x 9m	9.4 x 5.8m
Beam Section	0.19 x 0.23 m	0.23 x 0.30 m	0.27 x 0.37 m	0.19 x 0.23 m	0.27 x 0.37 m
Column Section	0.23 x 0.23 m	0.23 m dia.	0.26 x 0.26 m	0.23 x 0.23 m	0.26 x 0.26 m
Slab Section	0.1 m	0.1m	0.1m	0.1m	0.1m

Table 3.1 General Building Description

3.1.3 Preparation of As-Built Architectural Drawing

During the site visit, measurements were taken to prepare the as-built architectural drawings. The architectural drawing of the Model 1 prototype is shown below. Other architectural drawings can be found in the Appendix-B.

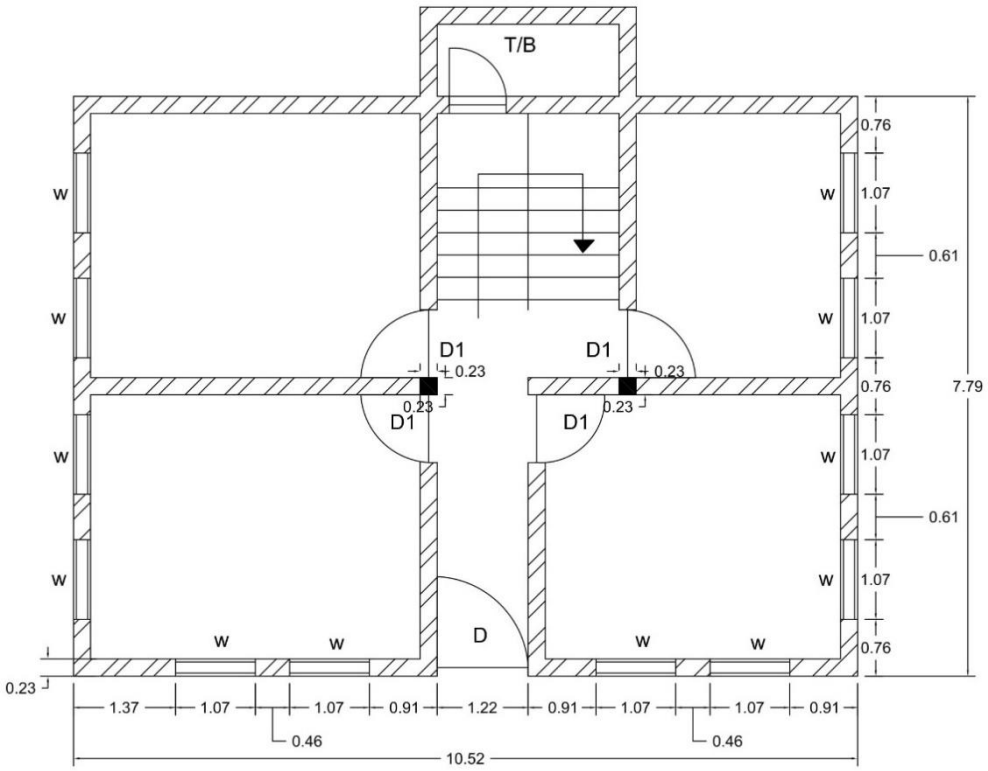

Figure 3.3 Floor plan

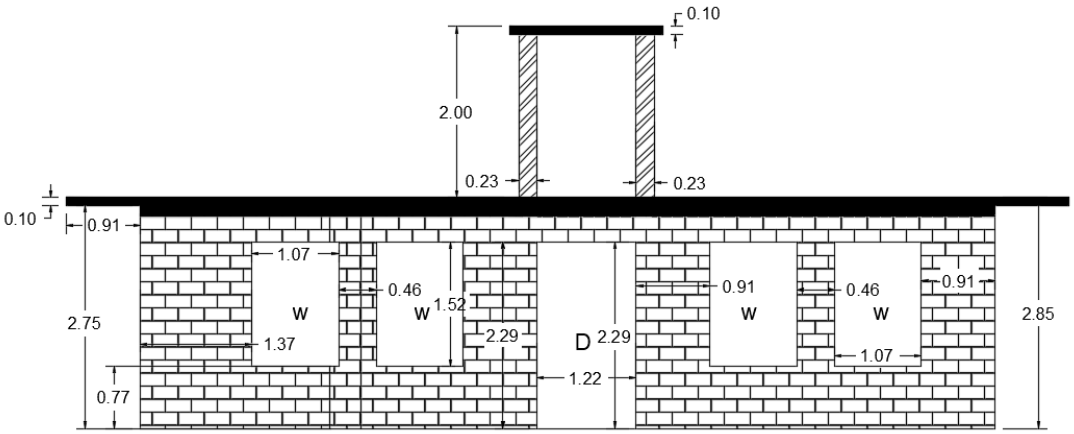

Figure 3.4 Elevation view

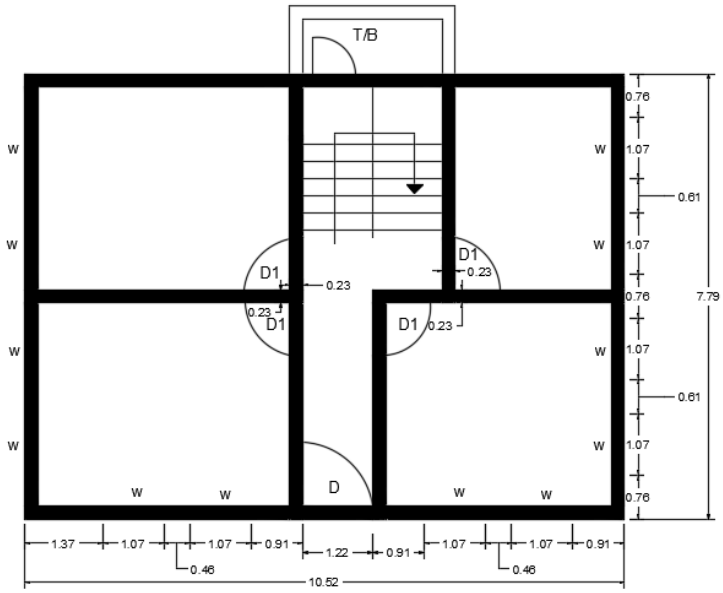

Figure 3.5 Beam layout plan

3.2. Model Validation for Use of Non-Linear Links

Andres Lepage and Reynaldo E. Sanchez (2011) proposed two modeling techniques for practical nonlinear static analysis: the Nonlinear Layer Model and the Nonlinear Link Model, which were used to support the development and application of a new Limit Design method for special reinforced masonry shear walls. The area elements at potential critical yielding sections in the Nonlinear Layer model are modified with specific layer definitions that account for material nonlinearity. The area elements at potential critical yielding sections are replaced with nonlinear links in the Nonlinear Link model. The proposed simplified models are described in their work by implementing them to a planar 2D one-story wall with two openings (fig. 3.6). Three vertical wall segments are joined to three joint segments by two horizontal wall segments in the model. At the roof level, the perforated wall structure is expected to have a rigid diaphragm situated 2'-0" below the top of the wall. Potential hinge locations are considered at ends of vertical and horizontal wall segments.

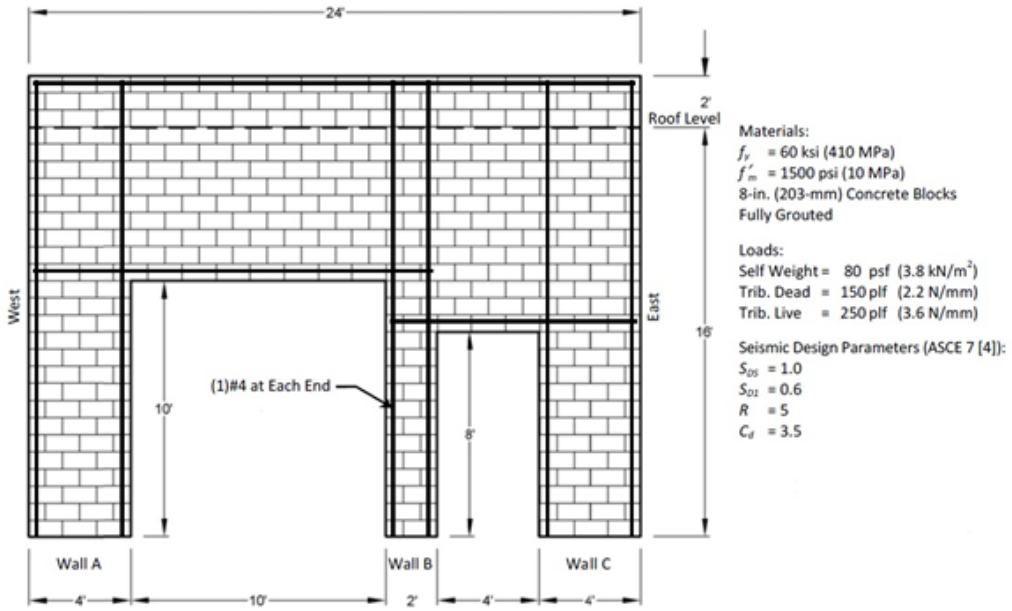

Figure 3.6 Description of wall considered, after Lepage et al. (2011).

The methodology offered by Lepage and Sanchez in their second method is the focus of this thesis. The area elements representing the interface of wall segments, where yielding is anticipated to occur, are substituted by nonlinear links defined as Multilinear plastic in the Nonlinear link model proposed in the research. The yielding wall segments' axial and in-plane shear behavior is represented by the user-defined force-deformation relationship. Outside of the predicted yielding zones, linear-elastic area elements with full gross section properties are used to simulate the area elements. A gravity load scenario is described as a pre-load condition in nonlinear static analysis to establish the beginning points on the force-deformation curves of each nonlinear link.

In this thesis, for accounting the non-linearity in the structure, the methodology proposed by Reynaldo and Sanchez in their second type of model i.e, the nonlinear link model has been followed. The area elements representing the interface of wall segments, where yielding is expected to occur, are substituted by nonlinear links defined as Multilinear plastic links in the nonlinear link model proposed in the study.

Reynaldo E. Sanchez's pushover curves for the Nonlinear Link Model, which is pertinent to our scenario, are compared to the pushover curves developed in this thesis.

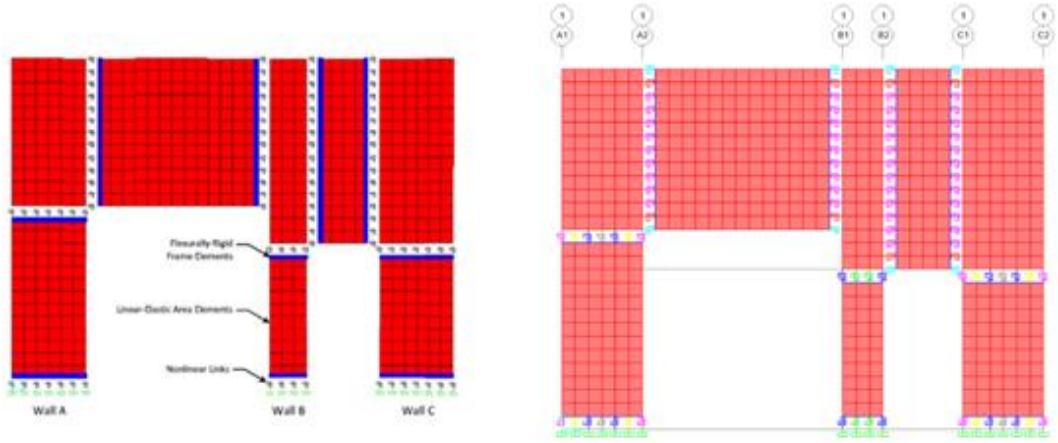

Figure 3.7 (a) Nonlinear Link Model with links as Proposed by Lepage et. al (b) Model prepared in SAP2000.

The introduction of nonlinear links which would replace the area elements just like in the Reynaldo and Sanchez models were based on the visual assessment of the building under study. The links have been used in accordance with the observed crack patterns in the actual structure. Also, frame hinges have been used at RCC column and beam junctions. The use of links in combination with frame hinges made it possible to account for the nonlinearity of the masonry structure under earthquake loadings. After performing the pushover analysis in the model with links, the pushover curve obtained was found to be in good accordance with the pushover curves obtained by Reynaldo E Sanchez and Lepage for their “nonlinear link model” (fig 3.8 (a)).

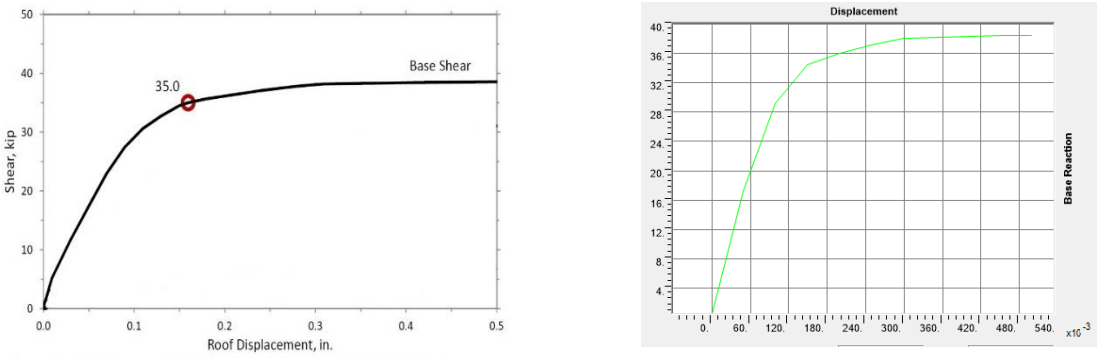

Figure 3.8 (a) Shear vs. Roof Displacement for Nonlinear Link Model, Eastward Loading, Lepage et al.(2011), (b) Pushover Curve (Shear vs Roof displacement) obtained from SAP 2000 V20.

3.3. Modelling of Building in SAP2000

The modelling and analysis are conducted in the Finite Element Software, SAP 2000 v20.0.0. wherein 3D macro-modelling approach is adopted to model the current building under study i.e., micro-modelling hasn't been done for the mortar joints and masonry units. The masonry wall elements are modelled as thick shell and the roof slabs as thin shell area elements. The nonlinearities in the masonry wall system are represented by the use of non-linear link elements. The use of NL links was validated through previously published literature. The validated modeling technique was adopted to develop the FE model of the selected building typology.

The structural members of the model include the centrally placed RCC column elements and beams which are modelled as frame elements. The peripheral walls as well as internal walls with thicknesses as specified in Table 3.1 are constructed in brick masonry in cement mortar. The roof slab and stair cover slab are 100mm thick. For proper transmission of the loads from area-to-area element, meshing of the area elements is done, the mesh size being 0.25m*0.25m. Because of lack of actual field data and material testing, all mechanical properties of materials in the building are taken from relevant past literatures that account for the present study. The foundation is assumed to be rigidly fixed at ground level and plinth level beams haven't been considered in modelling.

The representative FE model of first building model has 2250 numbers of thick shell elements, 1203 numbers of thin shell elements, 9 numbers of frame element and 363 numbers of NL links. The materials properties of masonry and RCC are obtained adopted from Phaiju et al. (2018).

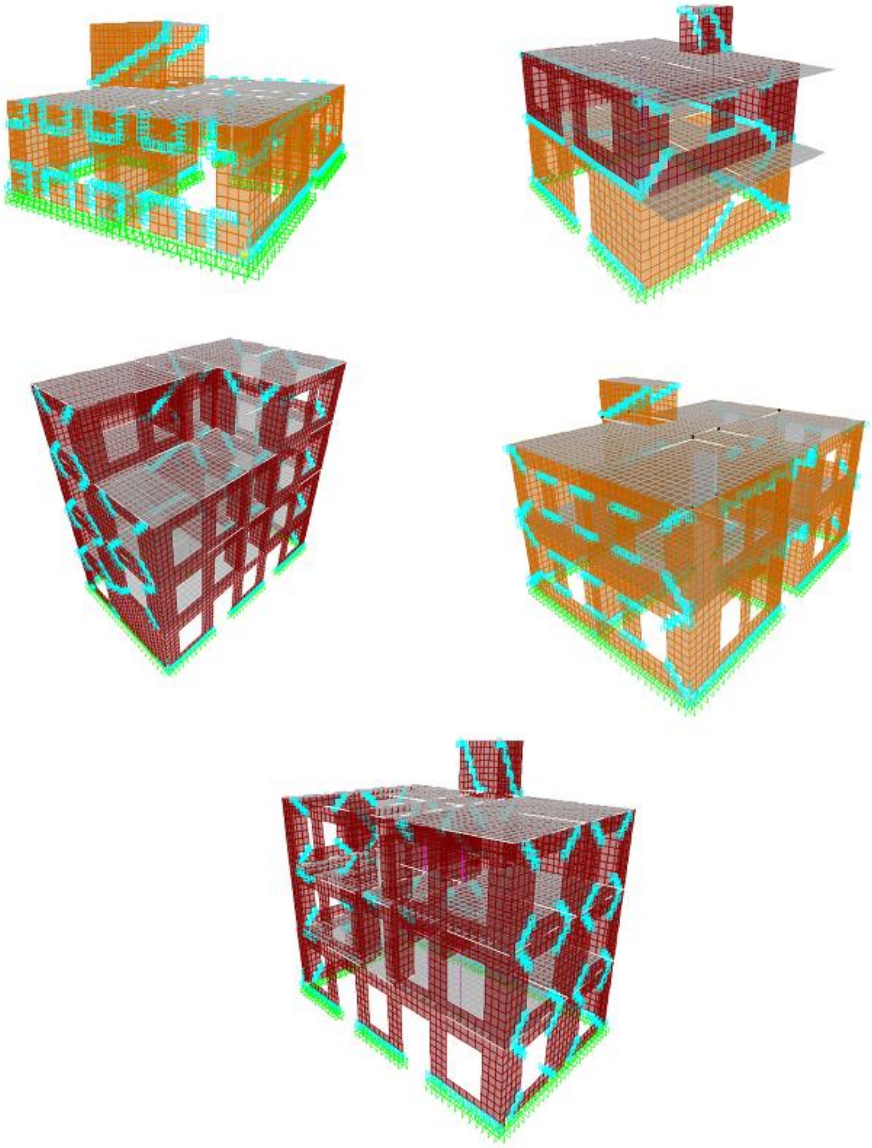

Figure 3.9 SAP2000 Model of Buildings considered

The different aspects which are important during modeling of the structure in SAP are enlisted below.

3.3.1. Material Properties

3.3.1.1. Concrete

Concrete grade for Beams/ Floor/ Roof slab	M20 (20MPa)
Young's Modulus ($E = 5000\sqrt{f_{ck}}$)	22 GPa
Poisson's Ratio	0.2

Table 3.2 Concrete Properties

3.3.1.2. Brick masonry in cement mortar (BCM)

Compressive Strength of Masonry	2.5 MPa
Young's Modulus	2703.2 MPa
Poisson's ratio	0.32
Modulus of Rigidity	915.1 MPa
Shear Strength	0.25 MPa

Table 3.3 BCM properties (Source: Phaiju et. al (2018))

3.3.2. Link Elements

The Link element is used to link together two joints. According to the types of attributes assigned to that element and the type of analysis being performed, each link element can exhibit up to three different forms of behavior: linear, nonlinear, and frequency-dependent (SAP2000 Manual, 2016).

The behavior of the link element can be defined by a set of structural properties known as link property. The relationship between force and displacement/deformation for the six internal deformations is specified in terms of link property.

The link properties may be broadly classified as

- Linear/Nonlinear
- Frequency-dependent

We are concerned with the use of Linear/ Nonlinear property sets for linear analysis followed by nonlinear analysis of the structure. The Multi-linear Plastic Property is employed in the model to simulate the structure's linear and nonlinear behavior.

Link parameters:

The initial stiffness was calculated from the linear-elastic response of the wall materials' gross-section characteristics. The force-deformation relationships assigned to nonlinear links (defined as Multilinear Plastic) to describe both axial and shear behavior.

The axial behavior of the link is defined by its longitudinal direction, whereas the shear behavior is defined by its in-plane transverse direction. The force vs. deformation data is dependent on the tributary area of the wall. The nonlinear links' axial response characteristics directly govern the wall's flexural behavior (Sánchez Bravo, 2012).

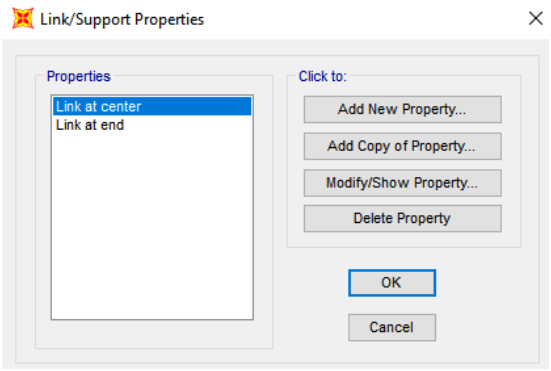

Figure 3.11 Link Properties definition

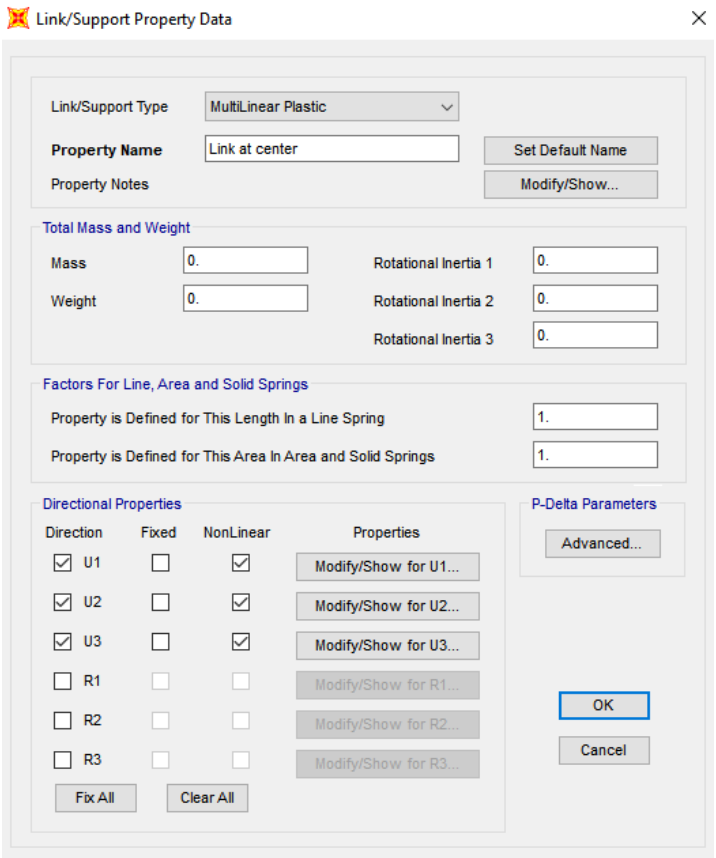

Figure 3.10 Link property data

Properties of link at interior points of wall:

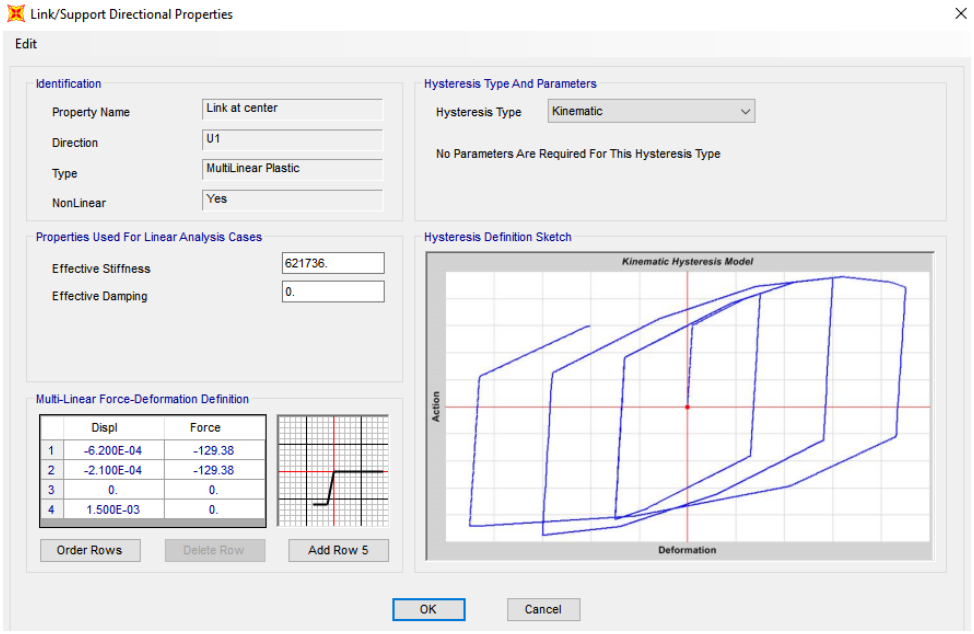

Figure 3.12 U1 (Axial dof for hinge located at interior points of wall)

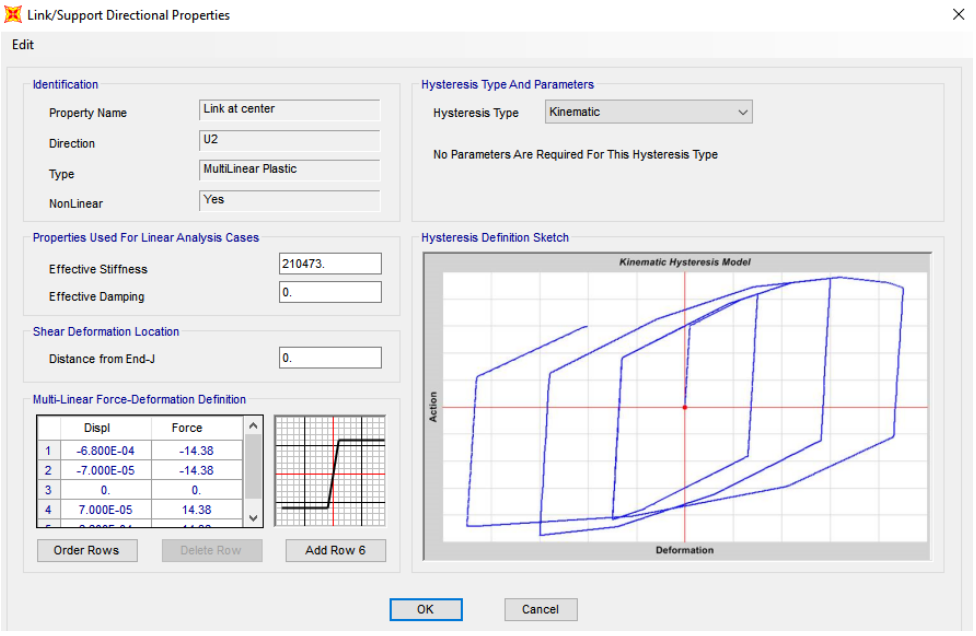

Figure 3.13 U2 (Shear dof for hinge located at interior points of wall)

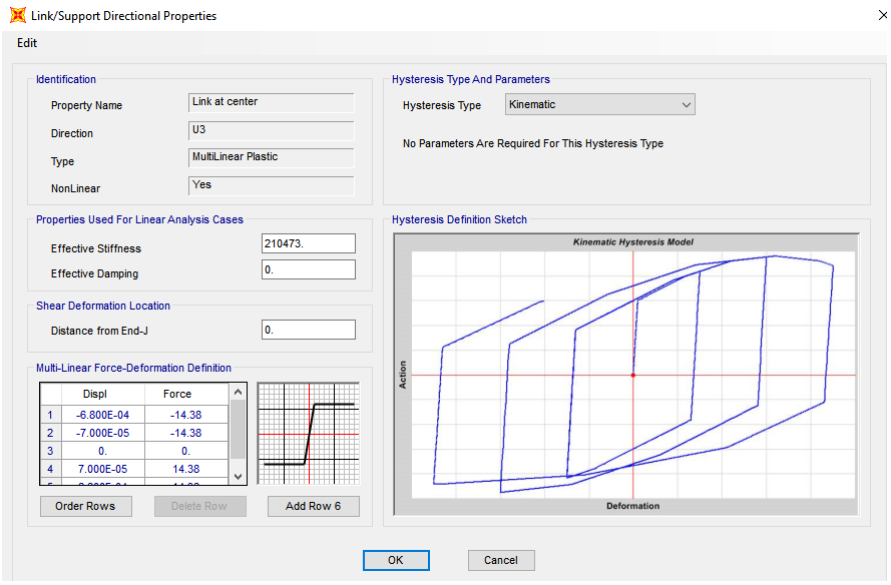

Figure 3.14 U3 (Shear dof for hinge located at interior points of wall)

Properties of masonry		
Young's Modulus of Elasticity (E) =	2703.2	MPa
Compressive strength of masonry (fm) =	2.5	MPa
Poisson's ratio (ν) =	0.32	
Density of masonry (γ) =	20	KN/m^3
Modulus of Rigidity (G) =	915.1	MPa

Calculation for links at interior points of wall

Assumptions:

Compressive stress = 0.9 * fm

Tensile stress = 0.

Bilinear material stress-strain plot:

Strain	Stress
-0.002497041	-2250
-0.000832347	-2250
0	0
0.006	0

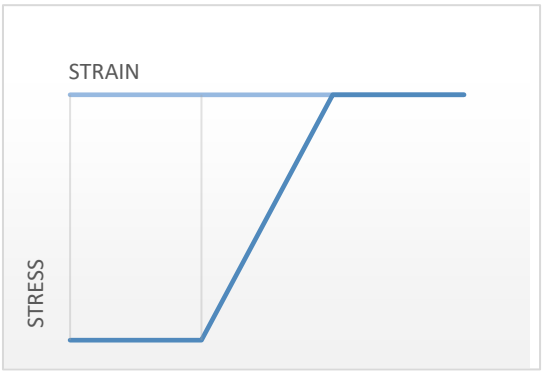

Where E = maximum stress/ corresponding strain = 2250/0.000832347= 2703200

Link properties for Axial direction(U1):

Size of mesh = L * H = 0.25 * 0.25m

Width of link (B) = 0.23m and Length of link = 0.25m

Cross sectional area of link (A trib)

= L * B [for vertical links, horizontally placed along length]

= B * H [for horizontal links, vertically placed along length]

Thus, A trib = 0.25 * 0.23 = 0.0575 m^2

Axial Force - Displacement Plot: Bilinear

Displacement	Force
-0.00062426	-129.375
-0.000208087	-129.375
0	0
0.0015	0
Stiffness=	621736

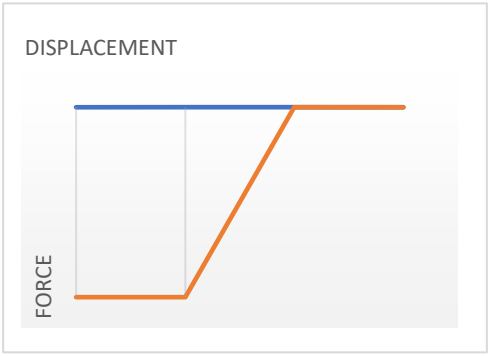

Link properties for Shear direction (U2 and U3):

Shear stress = 0.25 MPa

Shear strain = Shear stress/ G = 0.000272

Shear Force - Displacement Plot: Bilinear

Displacement	Force
-0.00068	-14.38
-0.00007	-14.38
0	0
0.00007	14.38
0.00068	14.38
Stiffness =	210473

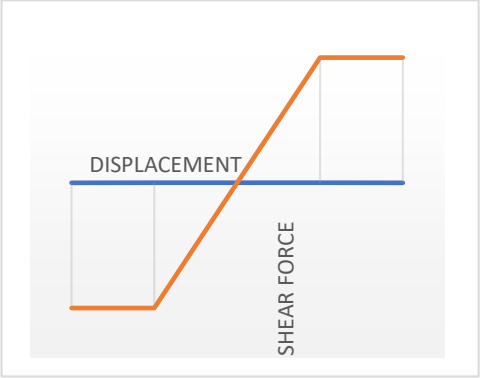

Properties for link at edges of wall:

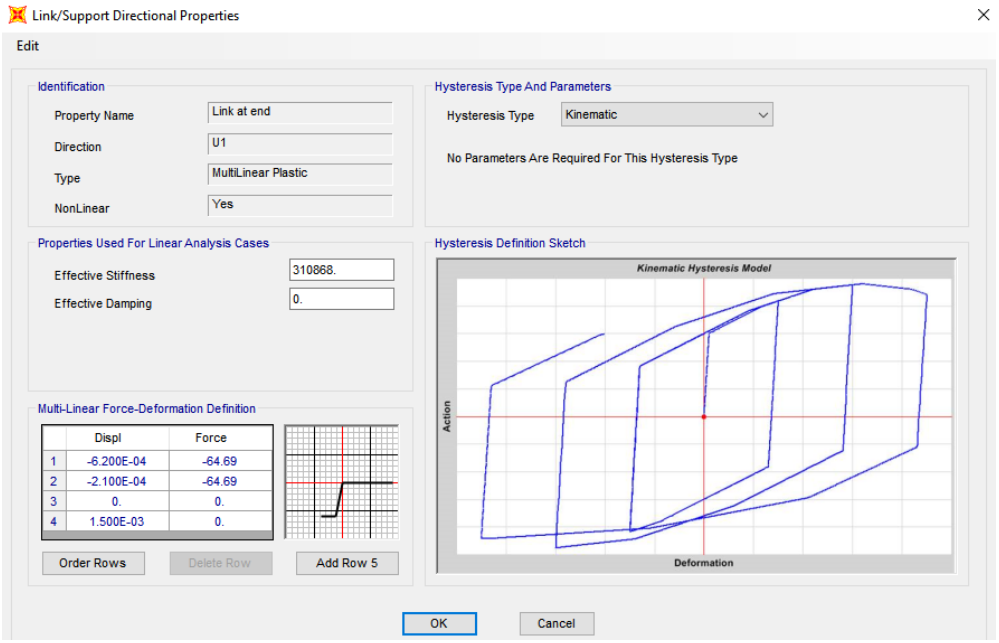

Figure 3.15 U1 (Axial dof for hinge located at edges of wall)

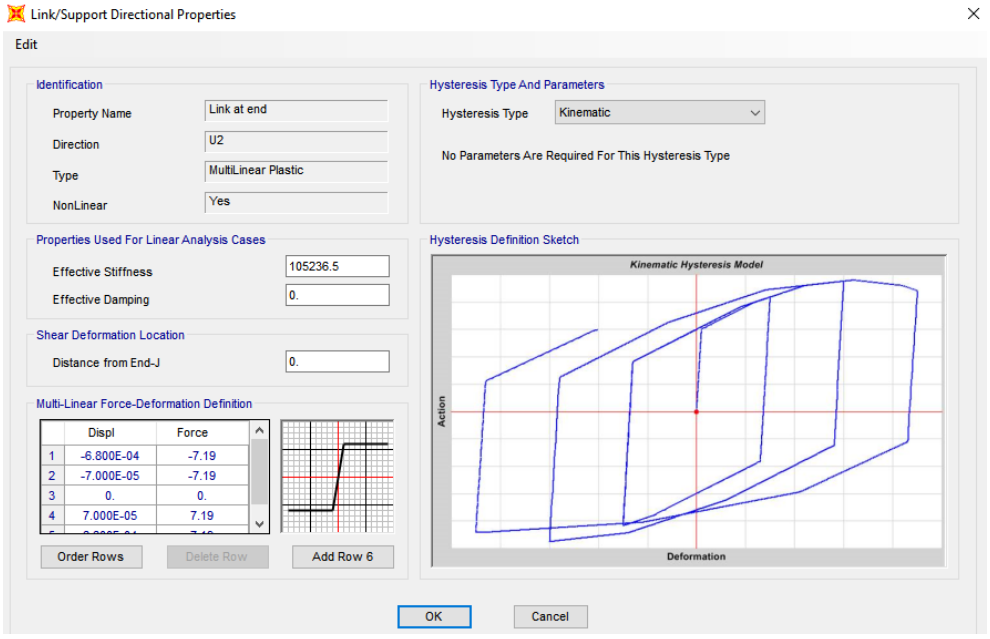

Figure 3.16 U2 (Shear dof for hinge located at edges of wall)

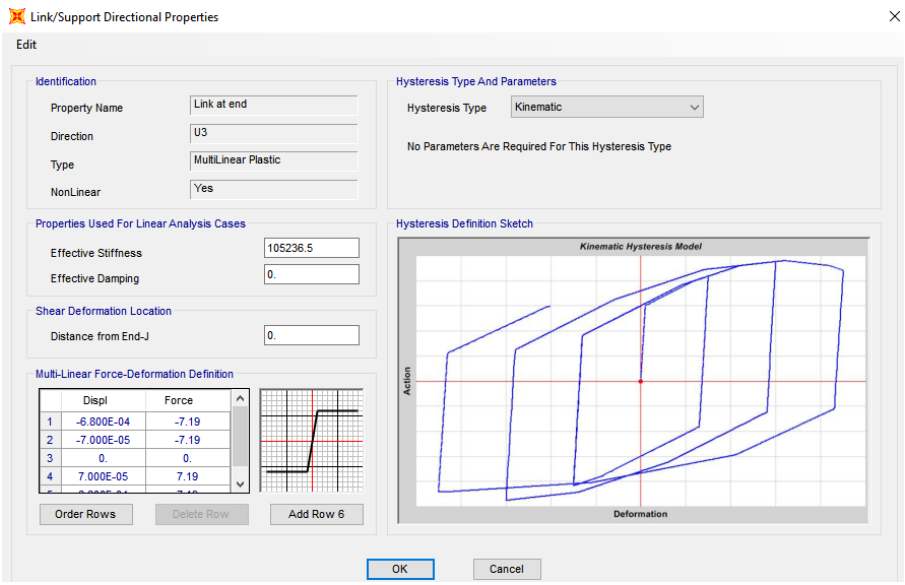

Figure 3.17 U3 (Shear dof for hinge located at edges of wall)

Calculation for links at edges of wall

Assumptions:

Compressive stress = 0.9 * fm

Tensile stress = 0.

Bilinear material stress-strain plot:

Strain	Stress
-0.002497041	-2250
-0.000832347	-2250
0	0
0.006	0

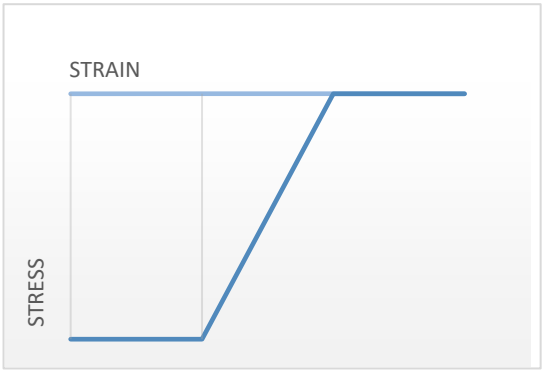

Where E = maximum stress/ corresponding strain = 2250/0.000832347= 2703200

Link properties for Axial direction(U1):

Size of mesh = L * H = 0.25 * 0.25m

Width of link (B) = 0.23m and Length of link = 0.25m

Cross sectional area of link (A trib)

= L * B [for vertical links, horizontally placed along length]

= B * H [for horizontal links, vertically placed along length]

Thus, A trib = ½ * 0.25 * 0.23 = 0.02875 m^2

Axial Force - Displacement Plot: Bilinear

Displacement	Force
-0.00062426	-64.6875
-0.000208087	-64.6875
0	0
0.0015	0
Stiffness=	310868

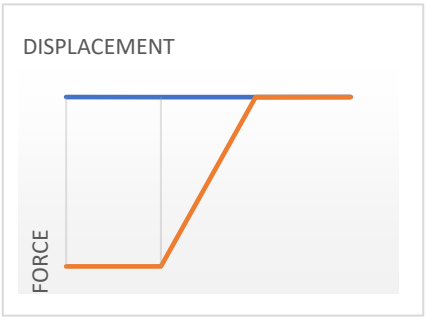

Link properties for Shear direction (U2 and U3):

Shear stress = 0.25 MPa

Shear strain = Shear stress/ G = 0.000272

Shear Force - Displacement Plot: Bilinear

Displacement	Force
-0.00068	-7.19
-0.00007	-7.19
0	0
0.00007	7.19
0.00068	7.19
Stiffness =	105237

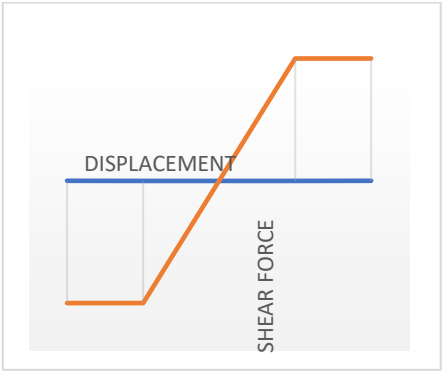

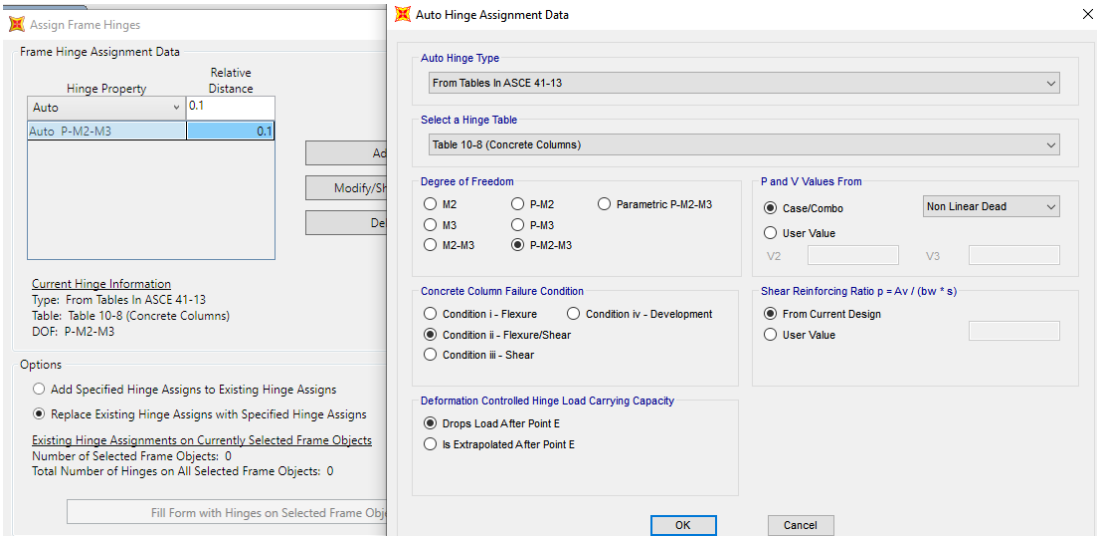

Figure 3.18 Frame hinges assignment (Column P-M2-M3 hinges and Beam M3 hinges) placed at 0.1 and 0.9 relative distances

Position of links:

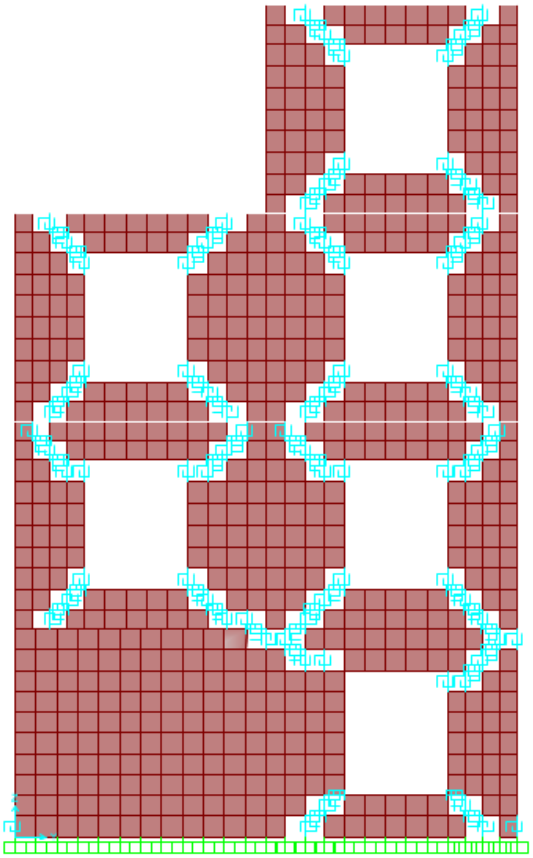

Figure 3.19 In-plane Links

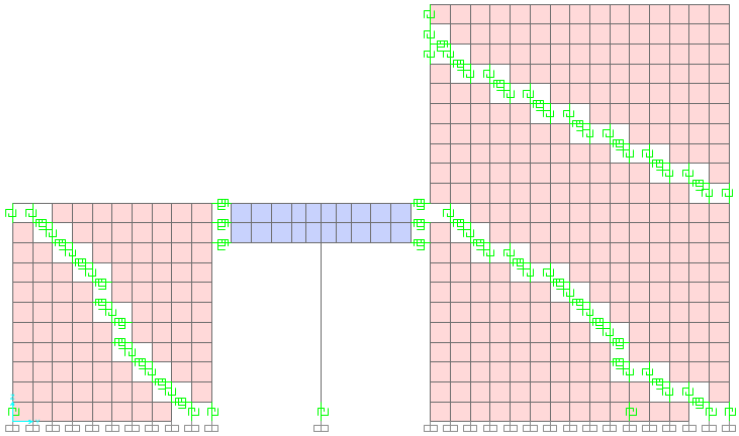

Figure 3.20 In-plane links along diagonal

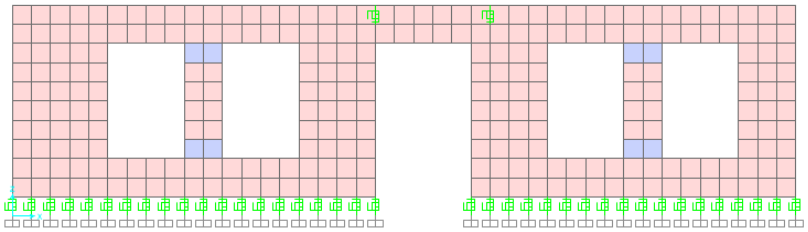

Figure 3.21 Out of plane links at toe

3.3.3. Design Loads

The unit weight of the materials for calculation of dead load is taken as:

Masonry walls: 20 KN/m^3

RCC Slabs: 25 KN/m^3

The different loads considered for the analysis of the building are shown in table below.

Design Load	**Type of Load**	**Self-Weight Multiplier**	**Auto Lateral Load Pattern**	**Remarks**
Dead	Dead	1		
Live	Live	0.25		Live Load on roof = 1.5 KN/m2

EQX	Quake	0	IS 1893:2016	Global X direction Importance factor (I)=1 Zone factor (Z) =0.36 Response reduction factor (R)=3
EQY	Quake	0	IS 1893:2016	Global Y direction Importance factor (I)=1 Zone factor (Z) =0.36 Response reduction factor (R)=3

Table 3.4 Loads considered during analysis

3.4. Nonlinear Static Analysis: Pushover Analysis

The building models are subjected to nonlinear static pushover analysis. For brevity and simplicity, pushover in Y direction is only presented in this thesis. This direction represents the weaker side of the buildings with presence of majority of openings along the in-plane loaded walls.

For the selected URM building Pushover analysis is performed by defining nonlinear load cases along the most vulnerable direction in both positive and negative directions. The following load case properties pertain to that for the first building model, presented here as an example.

Load Case Name	Remarks
Gravity	Load Case Type: **Static** Analysis Type: **Non linear** Initial Conditions: Zero Initial Conditions-Start from Unstressed State Modal Load Case: All Modal Loads Applied Use Modes from Case- **Modal** **Loads applied** Load Type: Load Pattern

	Load Name: Dead Scale Factor : 1 Load Type: Load Pattern Load Name: Live Scale Factor : 0.25 **Geometric Nonlinearity parameters**-None **Other Parameters** Load application: Full Load Results Saved: Final State Only Nonlinear parameters: Default
Push Y	Load Case Type: **Static** Analysis Type: **Non linear** Initial Conditions: Continue from State at End of Nonlinear Case – **Gravity** Modal Load Case: All Modal Loads Applied Use Modes from Case- **Modal** **Loads applied** Load Type: Load Pattern Load Name: EQY Scale Factor : 1 **Geometric Nonlinearity Parameters:** None **Other Parameters** Load application (for Model 1)

	Load Application Control- Displacement Control Control Displacement- Use Monitored Displacement- Load to a Monitored Displacement Magnitude of **0.05 m** Monitored Displacement- DOF **U2** at Joint 4884 Results Saved Results Saved- Multiple States For Each Stage Minimum Number of Saved States-150 Maximum Number of Saved States-200 Save positive Displacement increments only Nonlinear Parameters: Default

Table 3.5 Non-linear static analysis details

3.5. Capacity Spectrum Method (CSM)

After obtaining the Pushover curve, it is converted to the capacity spectrum of S_A versus S_D relationship represented by an Equivalent Single Degree of Freedom (ESDOF) System.

$$S_A(T) = \frac{V_B}{M} \text{ ..... (1)}$$

Where, V_B represents the seismic base shear, and M is the effective modal mass given by:

$$M = \frac{L_n^2}{M_n} = \frac{(\sum m_i\{\delta_{i1}\})^2}{\sum m_i\{\delta_{i1}\}^2} \text{ ..... (2)}$$

Also,

$$S_D(T) = \frac{D_R}{\beta} = \frac{(\delta_{1i})^T [m] (\delta_{1i})}{(\delta_{1i})^T [m] (1)} \text{ ..... (3)}$$

Where, displacement vector of first mode is given by: $\{\delta\}_1 = \{\Phi\}_1\beta_1 S_D(T)$ …… (4)
And, [m] is the lumped floor mass matrix.

Similarly, the input response spectrum curves in S_A - T, resulting from input parameters of certain earthquake intensity, is converted to Acceleration-Displacement Response Spectrum (ADRS) i.e. S_A - S_D plot by the relation:

$$S_D(T) = \left(\frac{T}{2\Pi}\right)^2 S_A(T) \text{ …… (5)}$$

With the demand spectrum and capacity curve in the same domain of spectral acceleration and spectral displacement (ADRS format), the CSM analysis follows the following stepwise procedures as proposed by Otani et al.(2000):

1. We decide the first yield point of the structure under consideration. In this study, the yield point corresponds to the spectral displacement (D_y) when the storey drift ratio reaches 0.1%.
2. Assume, the ductility, μ = 1, tangential to the spectral displacement axis on the capacity spectrum for the decided first yield point.
3. Now, we draw the line of equivalent stiffness, passing through the origin and this point.
4. The first plot of the performance point is found out, which is the point of intersection of the demand spectrum and the line of equivalent stiffness, μ = 1.
5. Now, changing the ductility factor, μ = 1.5, we locate the second point on the capacity curve, equivalent to multiplying factor times (n) to the first yield displacement (D_y). The multiplying factor corresponds to the ductility factor, which describes the limit states of the structure.
6. We draw the second line of equivalent stiffness which passes through the origin to the second point.

The equivalent damping ratio, h_e , is calculated from the following empirical formula:

$$h_e = 0.25 \left(1-\frac{1}{\sqrt{\mu}}\right)+ 0.05 \text{ …… (6)}$$

h_e for first mode is assumed as 0.05 for the damage-initiation limit state because structure behavior remains elastic at this stage.

7. Up to the damage initiation limit state, the demand spectra are created with a damping ratio of 5% and an equivalent damping ratio at the life safety limit state. The demand spectrum response reduction factor, Fh, is calculated using the following formula:

$$F_h = \frac{1.5}{1+10\, h_e} \text{ …… (7)}$$

8. Now we draw the reduced demand spectrum by multiplying both parameters by S_A and S_D by F_h.
9. Now, we find the second performance point which is the point of interaction of the demand spectrum and line of equivalent stiffness, μ =1.5.
10. We repeat the steps 5 to 10, and collect all the performance point with different ductility factors which gives the demand curve.
11. The interaction of the obtained demand curve and the capacity curves provides the final performance points.
12. A single performance point is obtained for one PGA level of the particular earthquake spectrum. A similar procedure is followed to obtain performance points for different PGA levels of different sources of earthquake response spectra.

A sample example for the determination of performance point for first building model with PGA 0.2g and 0.3g of NBC 105:2020 for hard soil response spectrums is shown in fig. 3.22. The performance points derived for rest of the models can be found in Appendix-C.

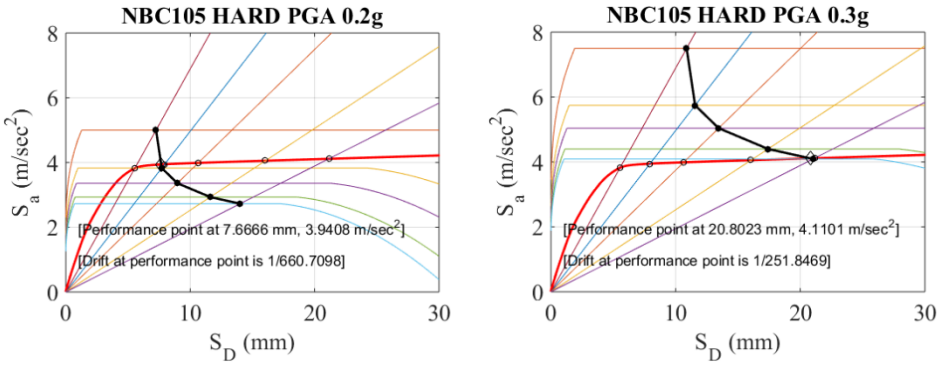

Figure 3.22 Determination of performance point using CSM (a) For PGA of 0.2g , (b) For PGA of 0.3g of NBC 105:2020

3.6. Fragility Curve

The CSM analysis for various ground motion parameters gives us a set of different values of performance point. These results can be correlated to a damage state, expressing the vulnerability of a structure to a user-defined intensity measure, as a graphical function of capacity curve. This fragility curve expresses the probability of exceedance of a specified damage stage as a function of input earthquake intensity parameters like: PGA, PGV, S_A, etc. Three categories of limit states of: Immediate

Occupancy (IO), Life safety (LS) and collapse prevention (CP) is defined for the generation of fragility curves. The different threshold values are assigned for the target structure from the structural capacity viewpoint at:

Immediate Occupancy (IO) = $^{1}/_{750}$ (i.e. 0.13%)

Life safety (LS) = $^{1}/_{500}$ (i.e. 0.2%)

Collapse Prevention (CP) = $^{1}/_{250}$ (i.e. 0.4%)

For present study, methodology proposed by Wen et al. (2004) is used for the generation of fragility curves. The probability that the structure exceeds the limit-damage state for the given ground motion intensity is provided by:

$$P(LS_i/GMI) = 1 - \emptyset \left(\frac{\lambda^{i}_{CL} - \lambda_{D/GMI}}{\beta_{D/GMI}}\right) \ldots\ldots\ldots (8)$$

Where the mean and standard deviation parameters are defined by:

$$\lambda_{D/GMI} = \ln(a_1) + a_2 \ln(GMI) \ldots\ldots\ldots (9)$$

$$\beta_{D/GMI} = \sqrt{\frac{\sum_{k=1}^{n}[LN(GMI_k) - \lambda_{GMI}(GMI_k)]^2}{n-2}} \ldots\ldots\ldots (10)$$

The constants a_1 and a_2 are obtained through linear regression analysis as the logarithmic plot of storey drift and Ground Motion Intensity (GMI) parameters in terms of PGA.

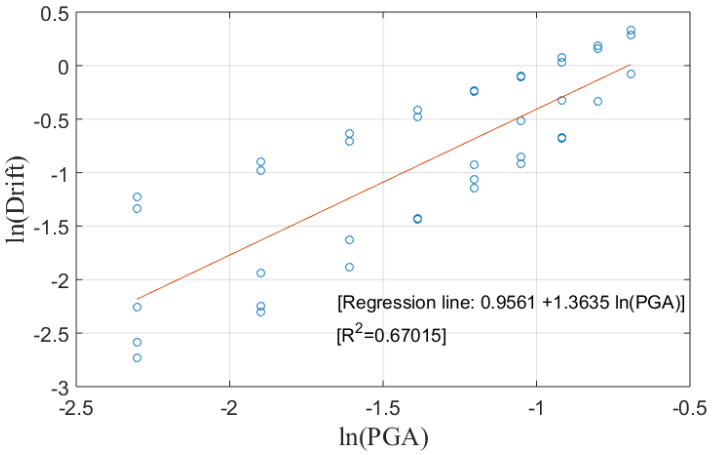

Figure 3.23 Regression plot ln(drift) vs ln(PGA)

A series of input parameters from different earthquake scenarios are provided, to obtain the linear plot, which gives us the threshold value. The fragility curves plots the probability of exceeding this threshold value corresponding to the categories of user-defined limit states. The fragility curve obtained after the input parameters from the earthquake scenarios with different values of PGA from NBC 105:2020 is shown in fig. 3.24.

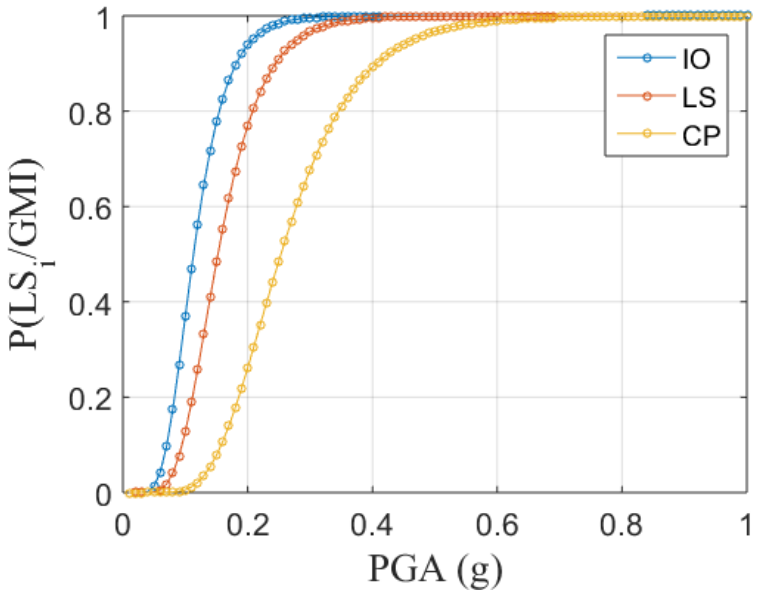

Figure 3.24 Fragility Curve

3.7. Seismic Strengthening Techniques: Retrofitting

When an assessment of the building indicates that the strength available before the damage was insufficient, and restoration alone will not be sufficient in future quakes, retrofitting is an improvement over the original strength. (Seismic Retrofitting Guidelines in Nepal: Masonry, MOUD, 2016)

Basic vulnerability elements to the seismic performance of the building in future earthquakes include the building system, configuration, and lateral force resisting system. Buildings can be retrofitted to address seismic weaknesses.

The seismic behavior of ancient existing structures is affected by structural inadequacies, material degradation over time, and adjustments made during use over time such as making new apertures, adding new pieces, and generating dissymmetry

in plan and elevation (Seismic Retrofitting Guidelines in Nepal: Masonry, MOUD, 2016).

(Retrofitting Guideline for developing Hazard Resilient Schools in Khyber Pakhtunkhwa, 2020) Retrofitting is done to improve the seismic safety of existing buildings that have been damaged by earthquakes, and must adhere to the local Seismic Building Code for:

- Increasing stiffness and/or increasing strength
- Increasing ductility
- Increasing the dissipation of energy
- Modify the nature of the ground motion transmitted to the building
- Base-isolation to reduce the earthquake force impact to buildings
- Reducing the exposure of the occupancy

Based on the damages observed in masonry buildings in the past earthquake and the deficiencies associated with it, the following strategies are applied in (Nepal Reconstruction Authority, Ready-to-use manuals for Repair and Retrofitting of Masonry Structures, 2021) regarding retrofitting.

- Configuration and load path improvement
- Wall-to-wall, wall-to-floor or wall-to-roof connection improvement
- Diaphragm improvements
- Roof improvements
- Bracing parapet walls
- Securing gable walls
- Capacity improvement of structural walls

(Nepal Reconstruction Authority, Ready-to-use manuals for Repair and Retrofitting of Masonry Structures, 2021) uses two major approaches in providing retrofitting solutions, viz Splint and Bandage and Strong back solution.

3.7.1. Splint and Bandage Approach

The splint and bandage approach consists of vertical splints at building corners, at wall intersections and on either side of openings, plus horizontal bandages at sill, lintel and floor levels. The wall areas not covered by the splints and bandages are covered by wire mesh that confines the walls.

Figure 3.25 Retrofitting with concrete and rebar Jacketing with splint-bandage and GI wire mesh (Brick masonry)

3.7.2. Strong back solution

The strong back design comprises a system of reinforced concrete strong backs placed at corners and at locations along the length of the wall, connected at the floor level by slab strips and a ring beam at the top of the walls. The strong back is connected to the walls with the help of through anchors. The function of the strong back is to brace the walls against out-of-plane forces, as well as to provide connectivity to the various elements of the system.

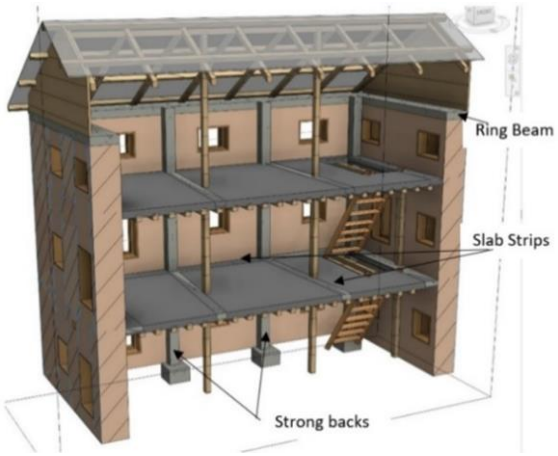

Figure 3.26 Strong back approach

4. RESULTS

4.1. Results from Linear Static Analysis

Following results were obtained from static analysis for the first model without links and with links. For the rest of the models, the results are included in Appendix-C.

Model 1					
Time period and Modal Participating Mass Ratios: Before using NL links					
Mode	**Period**	**UX**	**UY**	**SumUX**	**SumUY**
1	0.077689	0.17551	1.042E-05	0.17551	1.042E-05
2	0.060228	0.00044	0.68282	0.17595	0.68283
3	0.051982	0.00025	0.00855	0.1762	0.69138
4	0.047592	0.15623	0.00027	0.33243	0.69165
5	0.047482	0.04457	0.00084	0.37701	0.6925
6	0.043639	0.00034	0.00171	0.37735	0.69421
7	0.037579	0.41431	0.00294	0.79165	0.69715
8	0.031885	0.00704	0.05295	0.79869	0.75009
9	0.031542	0.00031	0.0177	0.799	0.76779
10	0.030218	8.267E-05	0.00824	0.79908	0.77603
11	0.029946	6.38E-06	1.051E-06	0.79909	0.77603
12	0.029572	0.00015	0.00043	0.79924	0.77646

Table 4.1 Time periods and modal mass participating ratios in plain model

Model 1					
Time period and Modal Participating Mass Ratios: After using NL links					
Mode	**Period**	**UX**	**UY**	**SumUX**	**SumUY**
1	0.08695	0.15743	0.00015	0.15743	0.00015
2	0.07417	0.00131	0.75966	0.15873	0.75981
3	0.06499	5.60E-08	0.012	0.15873	0.77182
4	0.05831	0.00294	0.00053	0.16167	0.77182
5	0.05587	0.13958	0.0011	0.30126	0.77182
6	0.05401	0.01292	0.00316	0.31418	0.77182
7	0.04926	0.00293	0.00378	0.3171	0.77182

8	0.04302	0.30797	0.00633	0.62508	0.77182
9	0.04066	0.07166	0.00212	0.69674	0.77182
10	0.03985	0.00562	0.00354	0.70236	0.77182
11	0.0391	0.09249	0.0036	0.79485	0.77182
12	0.03854	0.00153	0.00339	0.79639	0.77182

Table 4.2 Time periods and modal mass participating ratios after introduction of links

The fundamental time period and mass participating ratios are in good agreement with respect to both the models before and after the introduction of NL links.

4.2. Pushover Analysis

Pushover analysis was performed on the building with the monitored displacement being 0.4% of building height; monitored at roof level. This gave the following pushover curve for Base shear versus roof displacement for the first model.

Pushover results:

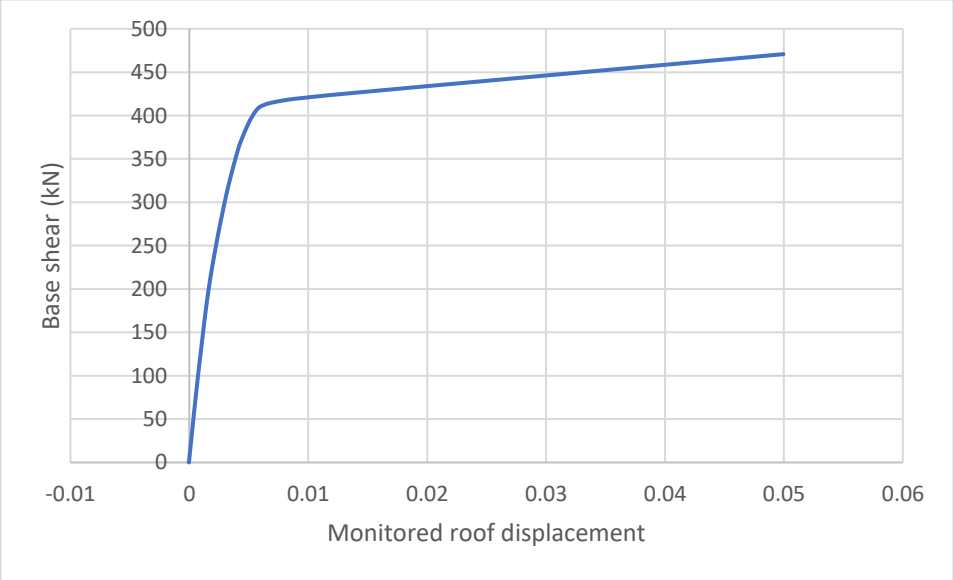

Figure 4.1 Base shear (kN) vs monitored displacement(m): (monitored at CG of roof for a displacement of 0.4% of building height)

4.3. Fragility Curves

The following fragility plot was obtained as follows for IO, LS and CP level.

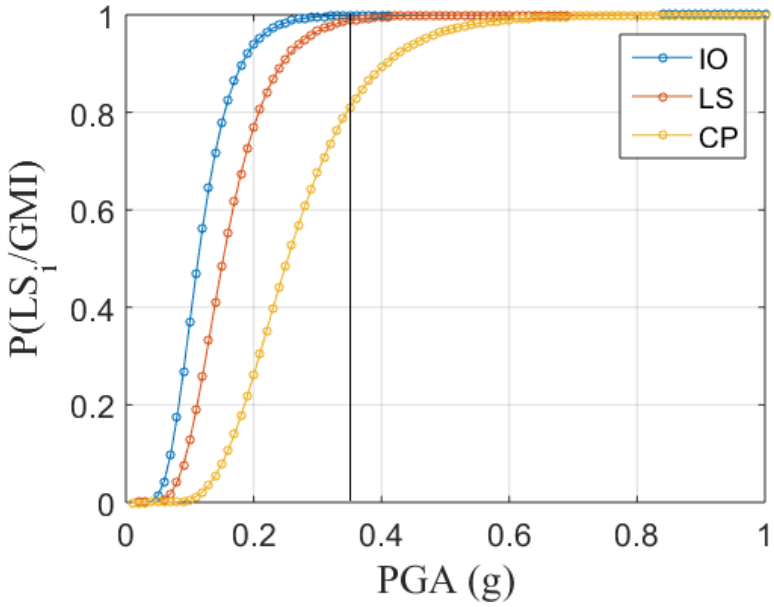

Figure 4.2 Fragility Curve

5. CONCLUSION AND RECOMMENDATIONS

5.1. Summary

This thesis work focused on assessing the vulnerability of the considered typology buildings in Panauti area. Firstly, a typical URM residential building typology was identified through survey. A detailed assessment of the buildings of selected typology was performed. The identified crack patterns and conventional crack patterns were taken into consideration to include the non-linearity in the structure. Non linearities were thus included by means of NL links placed at crack locations. Also, auto frame hinges were assigned for beams and columns. The FE model of three existing structures and remaining two fictious structures were generated and non-linear static pushover analysis was performed. The capacity curves from pushover analysis and demand curves from response spectrum of NBC 105:2020 for different PGA levels were used to obtain performance points of structures to corresponding demands. The array of performance points were used to further obtain the state of vulnerability through generation of fragility curves.

5.2. Conclusion and recommendations

The fragility curves were generated for different damage state levels with specified drift limits. The fragility curves generated depict the vulnerability of the considered structure to earthquake shakings. For a PGA of 0.36g (the Maximum Considered Earthquake (MCE) in IS 1893:2016), the probability of exceeding the CP level is 80% while exceeding the IO and LS level is 100%. High vulnerability of the considered typology structures is thus evident. Further, a greater number of buildings with similar typology can be analysed for getting a clearer picture of the state of vulnerability of these typology buildings. Accordingly, the future works will focus on extending the current model to propose seismic retrofitting measures for the selected prototype URM building. The following recommendations are made for future works.

1. Various retrofitting measures can be proposed according to the damage states.
2. The material properties for masonry can be determined experimentally for more accurate results.
3. Non-linear time history analysis can be used for development of fragility curves.

REFERENCES

Thapa, D. R., Tao, X., Wang, G., & Fan, F. (2017). Deterministic seismic hazard assessment for Nepal. In Sixteenth World Conference on Earthquake Engineering, Santiago, Chile, paper (Vol. 730, pp. 1-8).

Hendry, A. W., Sinha, B. P., & Davies, S. R. (Eds.). (2017). Design of masonry structures. CRC Press.

Marques, R., & Lourenço, P. B. (2011). Possibilities and comparison of structural component models for the seismic assessment of modern unreinforced masonry buildings. Computers & Structures, 89(21-22), 2079-2091..

Garbin, E., Galati, N., Nanni, A., Modena, C., & Valluzzi, M. R. (2007). Provisional design guidelines for the strengthening of masonry structures subject to in-plane loading. In Proceeding of tenth North American masonry conference (pp. 3-5).

Miha, T. (2006). Series on Innovation in structures and construction, Vol. 1: Earthquake-resistant design of masonry buildings, AS Elnashai and PJ Dowling.

ABK, A. (1984). Joint Venture," Methodology for mitigation of seismic hazards in existing unreinforced masonry buildings: The Methodology." Rep. ABK-TR-08.

Tiwari, K., Pradhan, S., Guragain, R., & Shrestha, H. Multiple analytical approaches on seismic retrofit design of unreinforced masonry buildings in Nepal.

Shrestha, H. D., Subedi, J., & Rajbhandari, M. (2016). Seismic retrofitting guidelines of buildings in Nepal. Kathmandu, Nepal: Government of Nepal, Ministry of Urban Development, Department of Urban Development and Building Construction.

Rai, D. C. (2005). Structural use of unreinforced masonry. IITK-GSDMA EQ, 12, 19.

FEMA-306, Evaluation of earthquake damaged concrete and masonry wall buildings US: Federal Emergency Management Agency.

FEMA-356, Pre-standard and commentary for the seismic rehabilitation of buildings. US: Federal Emergency Management Agency.

FEMA-273. NEHRP guidelines for the. Seismic rehabilitation of buildings US: Federal Emergency Management Agency.

ATC-40. (1996). Seismic Evaluation and Retrofit of Reinforced Concrete Buildings: Applied Technology Council.

ASCE 41-06, Seismic Rehabilitation of Existing Buildings; 2006.

ASCE Standard ASCE/41-13. (2014). American Society of Civil Engineers: Seismic Evaluation and Retrofit of Existing Buildings.

Ghiassi, B., Soltani, M., & Tasnimi, A. A. (2012). Seismic evaluation of masonry structures strengthened with reinforced concrete layers. Journal of Structural Engineering, 138(6), 729-743.

Caliò, I., Marletta, M., & Pantò, B. (2012). A new discrete element model for the evaluation of the seismic behaviour of unreinforced masonry buildings. Engineering Structures, 40, 327-338.

Andreini, M., Caliò, I., Cannizzaro, F., De Falco, A., Giresini, L., Pantò, B., & Sassu, M. (2014). Seismic assessment of the historical mixed masonry-reinforced concrete government Palace in La Spezia. Instituto de Ingeniería, UNAM.

P. B, Lourenço. (1996). Computational strategies for masonry structures, PhD Thesis, Delft University Press, Delft, The Netherlands.

Campbell, J., & Durán, M. (2017). Numerical model for nonlinear analysis of masonry walls. Revista de la Construcción. Journal of Construction, 16(2), 189-201.

SAP-2000. CSI analysis reference manual Berkeley, California, USA; 2016.

Sanchez, R. E. (2012). Limit Design of Reinforced Masonry Walls For Earthquake-Resistant Construction, PhD Thesis, Pennsylvania State University.

Khan, M. A. (2013). Earthquake-Resistant Structures: Design, Build, and Retrofit. Butterworth-Heinemann.

Freeman, S. A. (1998). The capacity spectrum method. In Proceedings of the 11th European conference on earthquake engineering, Paris (pp. 6-11).

Park, J., Towashiraporn, P., Craig, J. I., & Goodno, B. J. (2009). Seismic fragility analysis of low-rise unreinforced masonry structures. Engineering Structures.

Motra, G. B., & Paudel, S. (2021). Performance evaluation of strengthening options for institutional brick masonry buildings: A case study of Pulchowk Campus. Progress in Disaster Science.

Maharjan, A., & Parajuli, H. R. (2020). Seismic Performance Evaluation of Stone Masonry Houses Constructed with Reinforced Concrete Bands. Nepal Journal of Science and Technology, 19(1), 204-214.

Motra, G. B., Sah, B. K., & Jha, P. (2021). Structural condition assessment and retrofitting of Shital Niwas building (presidential palace). Progress in Disaster Science, 10, 100174.

Magenes, G., & Fontana, A. D. (1998). Simplified non-linear seismic analysis of masonry buildings. In Proc. Br. Masonry Soc. No. 8 (pp. 190-195).

Guragain, R., Dixit, A. M., & Meguro, K. (2012). Development of fragility functions for low strength masonry buildings in Nepal using applied element methods. 15th world conference of earthquake engineering, Lisbon, Portugal.

Chikanbanjar, M., Motra, G. B., & Maharjan, D. K. (2019). Non-linear Static Analysis of Unreinforced Masonry Building. Proceedings of IOE Graduate Conference.

Basukala, S. S., & Maskey, P. N. (2017). Seismic vulnerability of traditional masonry building a case study of Byasi, Bhaktapur. Journal of Science and Engineering.

Penelis, G. G. (2006). An efficient approach for pushover analysis of unreinforced masonry (URM) structures. Journal of Earthquake Engineering, 10(03), 359-379.

Borzi, B., Pinho, R., & Crowley, H. (2008). Simplified pushover-based vulnerability analysis for large-scale assessment of RC buildings. Engineering structures, 30(3), 804-820.

Tripathi, A., & Rai, D. C. (2019). Seismic vulnerability assessment and fragility analysis of stone masonry monastic temples in Sikkim Himalayas. International Journal of Architectural Heritage, 13(2), 257-272.

Butenweg, C. & Gellert, C. (2008). Displacement based design of masonry structures, Conference Proceedings: 14th International Brick & Block Masonry Conference Sydney, Australia.

Lepage, A., Dill, S., Haapala, M., & Sanchez, R. (2011). Seismic design of reinforced masonry walls: current methods and proposed limit-design alternative. In Proceedings, 11th North American Masonry Conference.

Wen, Y. K., Ellingwood, B. R., & Bracci, J. M. (2004). Vulnerability function framework for consequence-based engineering. MAE Center Report 04-04.

Build Change. (2015). April 25, 2015: Gorkha earthquake, Nepal: post-disaster reconnaissance report. Denver

National Planning Commission Nepal (NPC).2015. Post disaster need assessment. Kathmandu: Government of Nepal.

Vaculik, J. (2012). Unreinforced masonry walls subjected to out-of-plane seismic actions, PhD Thesis, The University of Adelaide.

Gautam, D., Fabbrocino, G., & de Magistris, F. S. (2018). Derive empirical fragility functions for Nepali residential buildings. Engineering Structures, 171, 617-628.

Yi, T. (2004). Experimental investigation and numerical simulation of an unreinforced masonry structure with flexible diaphragms. Georgia Institute of Technology.

D'Ayala, D., & Speranza, E. (2003). Definition of collapse mechanisms and seismic vulnerability of historic masonry buildings. Earthquake Spectra, 19(3), 479-509.

Phaiju, S., & Pradhan, P. M. (2018). Experimental work for mechanical properties of brick and masonry panel. Journal of Science and Engineering, 5, 51-57.

Ministry of Urban Development. (2016). Seismic Retrofitting Guidelines in Nepal: Masonry.

Nepal Reconstruction Authority. (2021). Ready-to-use manuals for Repair and Retrofitting of Masonry Structures.

UN HABITAT, Education Department, Government of Khyber Pakhtunkhwa. (2020). Retrofitting Guideline for developing Hazard Resilient Schools in Khyber Pakhtunkhwa.

Nepal Earthquake Retrofitting and Rehabilitation Standards. (2017). Nepal Health Sector Support Programme III.

National Planning Commission Nepal (NPC). (2015). Post disaster need assessment. Kathmandu: Government of Nepal.

APPENDIX- A

A1. Selected Building Typologies

The following real building models have been selected in the study besides two hypothetical models.

Figure: Building Model -1

Figure: Building Model-2

Figure: Building Model-3

A2. Damages and cracks seen in buildings considered

Following were some of the damages and cracks seen in building model-1.

Figure: Diagonal cracks from opening

Figure: Diagonal cracks from opening

Fig: Cracks from opening to opening

Fig: Cracks through pier

Fig: Cracks from opening

Following were some of the damages and cracks seen in building model-2.

Fig: Cracks from opening

Fig: Diagonal cracks from opening

Following were some of the damages and cracks seen in building model-3.

Figure: Diagonal cracks from opening

Figure: Diagonal cracks from opening

Figure: Cracks through pier

Figure: Diagonal cracks from opening

APPENDIX- B

B1. Architectural Drawings

The following architectural drawings have been prepared for various building models.

 # Model-2

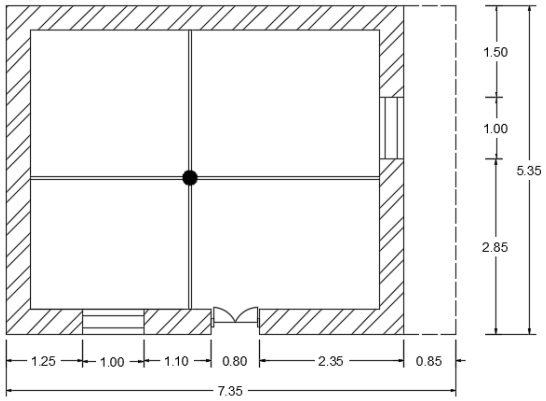

Figure: Ground floor plan

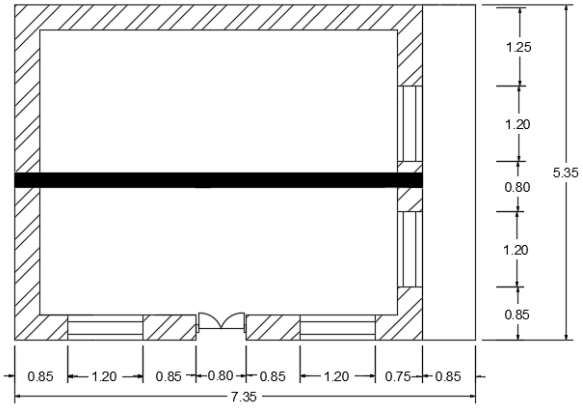

Figure: Beam layout plan

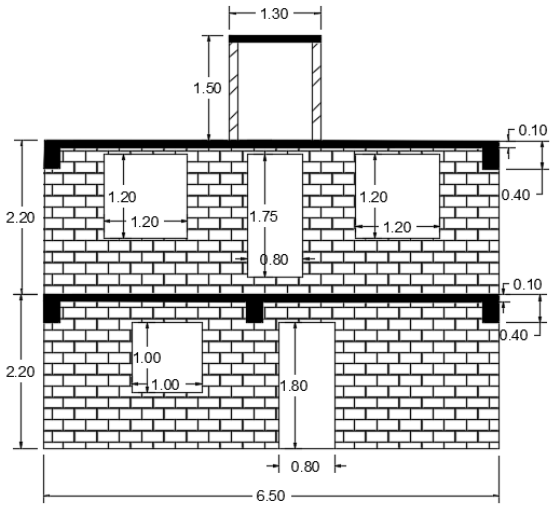

Figure: Elevation

#Model-3

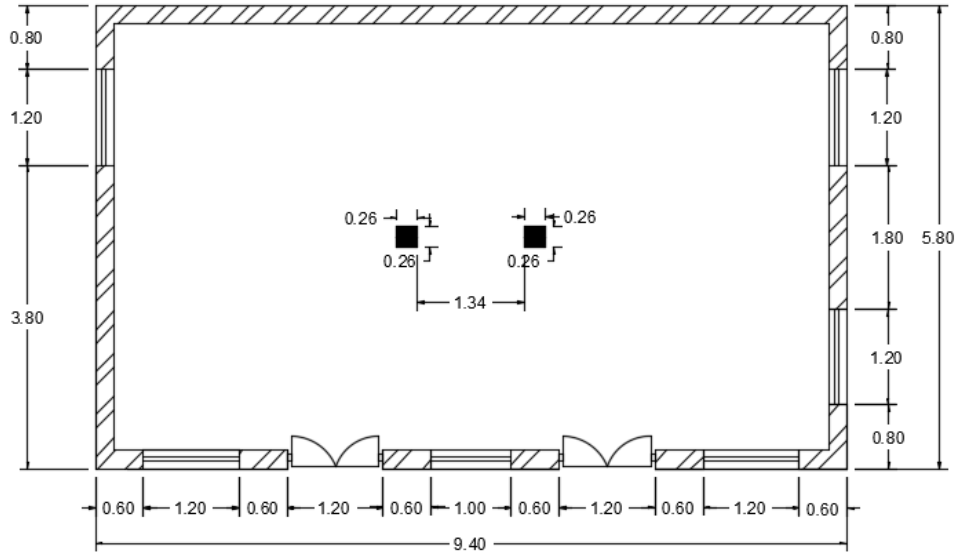

Figure: Ground floor plan

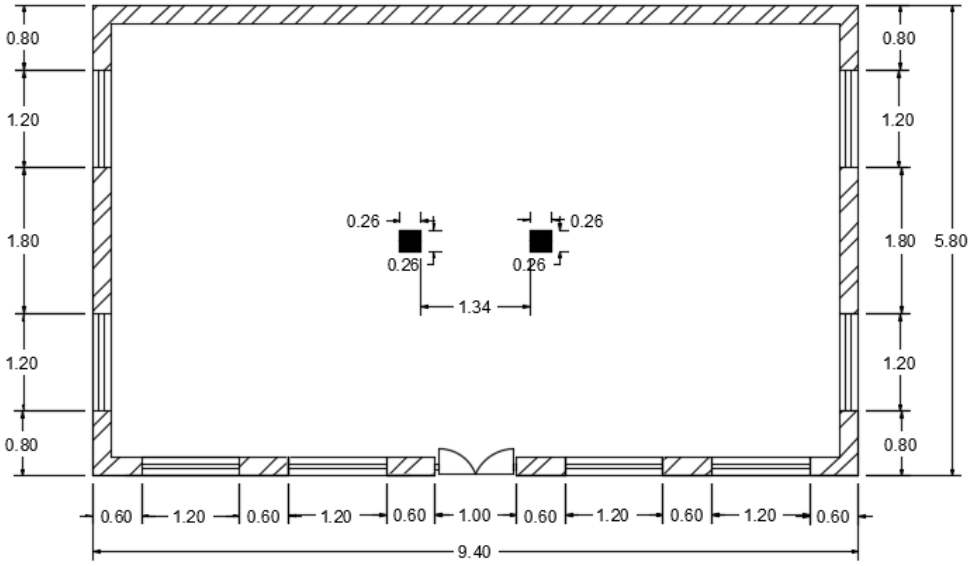

Figure: First floor plan

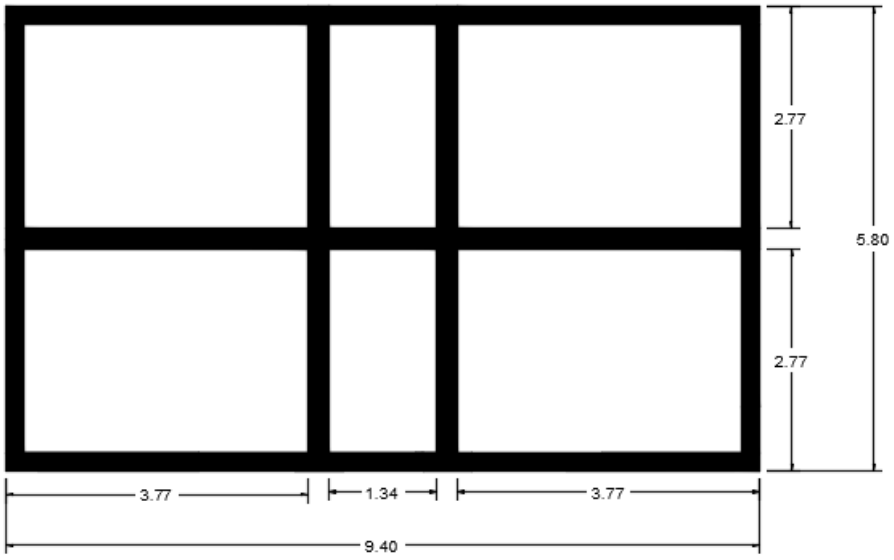

Figure: Beam layout plan

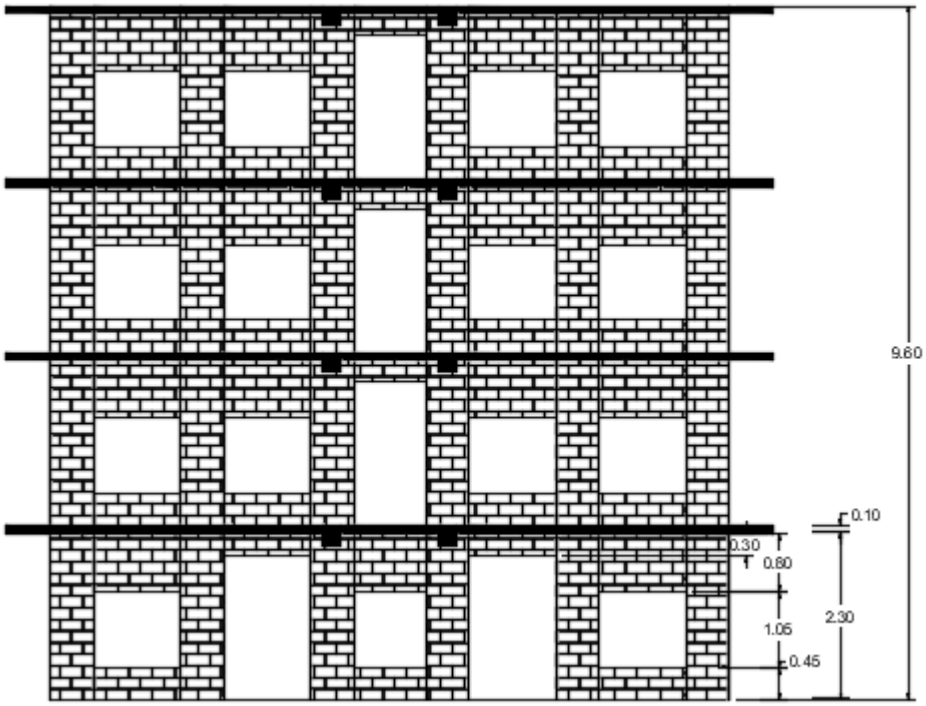

Figure: Elevation

APPENDIX- C

C.1 Results from static analysis

Model 1					
Time period and Modal Participating Mass Ratios: Before using NL links					
Mode	**Period**	**UX**	**UY**	**SumUX**	**SumUY**
1	0.077689	0.17551	1.042E-05	0.17551	1.042E-05
2	0.060228	0.00044	0.68282	0.17595	0.68283
3	0.051982	0.00025	0.00855	0.1762	0.69138
4	0.047592	0.15623	0.00027	0.33243	0.69165
5	0.047482	0.04457	0.00084	0.37701	0.6925
6	0.043639	0.00034	0.00171	0.37735	0.69421
7	0.037579	0.41431	0.00294	0.79165	0.69715
8	0.031885	0.00704	0.05295	0.79869	0.75009
9	0.031542	0.00031	0.0177	0.799	0.76779
10	0.030218	8.267E-05	0.00824	0.79908	0.77603
11	0.029946	6.38E-06	1.051E-06	0.79909	0.77603
12	0.029572	0.00015	0.00043	0.79924	0.77646

Model 1					
Time period and Modal Participating Mass Ratios: After using NL links					
Mode	**Period**	**UX**	**UY**	**SumUX**	**SumUY**
1	0.08695	0.15743	0.00015	0.15743	0.00015
2	0.07417	0.00131	0.75966	0.15873	0.75981
3	0.06499	5.60E-08	0.012	0.15873	0.77182
4	0.05831	0.00294	0.00053	0.16167	0.77182
5	0.05587	0.13958	0.0011	0.30126	0.77182
6	0.05401	0.01292	0.00316	0.31418	0.77182
7	0.04926	0.00293	0.00378	0.3171	0.77182
8	0.04302	0.30797	0.00633	0.62508	0.77182
9	0.04066	0.07166	0.00212	0.69674	0.77182
10	0.03985	0.00562	0.00354	0.70236	0.77182
11	0.0391	0.09249	0.0036	0.79485	0.77182
12	0.03854	0.00153	0.00339	0.79639	0.77182

Model 2					
Time period and Modal Participating Mass Ratios: Before using NL links					
Mode	**Period**	**UX**	**UY**	**SumUX**	**SumUY**
1	0.069994	0.13955	0.40074	0.13955	0.40074
2	0.060747	0.46596	0.19784	0.60551	0.59858
3	0.050597	0.00018	0.00116	0.60569	0.59975
4	0.042923	6.161E-05	0.00087	0.60575	0.60061
5	0.040648	0.00454	0.0017	0.61029	0.60232
6	0.037887	0.06613	0.05835	0.67642	0.66067
7	0.036635	1.082E-05	0.00541	0.67643	0.66608
8	0.033675	0.00656	0.00066	0.68299	0.66674
9	0.032604	0.00067	0.00129	0.68366	0.66802
10	0.031751	0.0011	0.00024	0.68476	0.66826
11	0.031321	0.00188	0.00082	0.68664	0.66908
12	0.029919	1.102E-09	0.02715	0.68664	0.69623

Model 2					
Time period and Modal Participating Mass Ratios: After using NL links					
Mode	**Period**	**UX**	**UY**	**SumUX**	**SumUY**
1	0.086802	0.01821	0.42545	0.01821	0.42545
2	0.072514	0.08531	0.07951	0.10352	0.50496
3	0.067519	0.48086	0.11544	0.58438	0.62041
4	0.05382	4.241E-05	0.00022	0.58442	0.62063
5	0.047905	0.00428	0.04838	0.5887	0.66901
6	0.046285	0.0001	0.00103	0.5888	0.67004
7	0.043	0.0046	0.00123	0.59341	0.67127
8	0.040837	0.08647	0.03545	0.67988	0.70672
9	0.037768	0.01283	0.0013	0.6927	0.70802
10	0.034365	0.00155	0.01025	0.69425	0.71826
11	0.034122	0.00338	0.05914	0.69763	0.77741
12	0.033769	2.153E-05	0.02525	0.69765	0.80266

Model 3					
Time period and Modal Participating Mass Ratios: Before using NL links					
Mode	**Period**	**UX**	**UY**	**SumUX**	**SumUY**
1	0.205023	0.12448	0.62522	0.12448	0.62522
2	0.176369	0.50593	0.19354	0.63041	0.81876
3	0.108113	0.1694	0.00953	0.79981	0.8283
4	0.069452	0.00779	0.01633	0.80759	0.84463
5	0.066382	0.02014	0.06779	0.82773	0.91243
6	0.063381	0.00014	0.001	0.82787	0.91343
7	0.062307	7.103E-05	1.002E-05	0.82794	0.91344
8	0.061789	0.02428	0.00236	0.85223	0.9158
9	0.061608	0.00817	0.00838	0.8604	0.92418
10	0.058656	0.04149	0.00783	0.90189	0.93201
11	0.045519	6.395E-05	3.387E-05	0.90195	0.93204
12	0.042681	0.00032	0.00286	0.90227	0.9349

Model 3					
Time period and Modal Participating Mass Ratios: After using NL links					
Mode	**Period**	**UX**	**UY**	**SumUX**	**SumUY**
1	0.224505	0.10718	0.65604	0.10718	0.65604
2	0.190585	0.50389	0.17543	0.61107	0.83147
3	0.115952	0.18286	0.00848	0.79393	0.83996
4	0.074257	0.00585	0.08576	0.79978	0.92572
5	0.071899	0.04985	0.00072	0.84962	0.92644
6	0.06831	0.00048	0.00137	0.85011	0.92781
7	0.066824	3.848E-06	0.00016	0.85011	0.92797
8	0.065984	0.03107	0.01175	0.88118	0.93972
9	0.064733	0.00181	4.355E-05	0.88299	0.93976
10	0.063265	0.00981	0.00291	0.8928	0.94267
11	0.057075	1.747E-05	0.00312	0.89282	0.94579
12	0.053989	0.00449	7.452E-05	0.89731	0.94587

Model 4					
Time period and Modal Participating Mass Ratios: Before using NL links					
Mode	**Period**	**UX**	**UY**	**SumUX**	**SumUY**
1	0.107976	3.479E-06	0.76151	3.479E-06	0.76151
2	0.090544	0.34658	2.028E-05	0.34658	0.76153
3	0.074325	0.3581	1.168E-06	0.70469	0.76153
4	0.056906	0.06936	4.868E-07	0.77404	0.76153
5	0.055203	6.505E-05	0.00017	0.77411	0.7617
6	0.054519	0.00966	6.456E-07	0.78377	0.7617
7	0.050205	2.899E-06	5.752E-05	0.78377	0.76175
8	0.049957	2.009E-07	2.663E-06	0.78377	0.76176
9	0.049124	3.977E-06	0.00033	0.78378	0.76208
10	0.048925	6.303E-05	0.0000384	0.78384	0.76212
11	0.046308	2.269E-05	0.0012	0.78386	0.76332
12	0.04619	0.00023	4.057E-05	0.7841	0.76336

Model 4					
Time period and Modal Participating Mass Ratios: After using NL links					
Mode	**Period**	**UX**	**UY**	**SumUX**	**SumUY**
1	0.110771	2.512E-08	0.79638	2.512E-08	0.79638
2	0.086891	0.26958	1.754E-07	0.26958	0.79638
3	0.068959	0.49181	1.817E-08	0.76139	0.79638
4	0.054661	1.472E-06	0.00013	0.76139	0.7965
5	0.054483	0.00046	2.16E-07	0.76185	0.7965
6	0.049844	1.816E-06	1.373E-05	0.76185	0.79652
7	0.049789	0.00171	3.412E-11	0.76356	0.79652
8	0.049399	8.295E-06	0.00051	0.76357	0.79702
9	0.049297	0.00187	2.15E-06	0.76544	0.79703
10	0.046625	1.722E-07	0.00096	0.76544	0.79799
11	0.046556	0.00105	7.007E-07	0.7665	0.79799
12	0.043891	0.02841	3.466E-10	0.79491	0.79799

Model 5					
Time period and Modal Participating Mass Ratios: Before using NL links					
Mode	**Period**	**UX**	**UY**	**SumUX**	**SumUY**
1	0.294688	6.158E-05	0.3114	6.158E-05	0.3114
2	0.152354	0.61587	0.00014	0.61593	0.31154
3	0.085216	0.19422	0.00013	0.81015	0.31167
4	0.075804	2.769E-07	9.738E-05	0.81015	0.31177
5	0.064173	0.0000465	0.44662	0.81019	0.75839
6	0.063429	3.378E-07	0.0174	0.81019	0.77579
7	0.062486	4.755E-06	1.368E-06	0.8102	0.77579
8	0.06082	0.00551	6.982E-06	0.81571	0.7758
9	0.058014	0.0000342	0.02155	0.81574	0.79735
10	0.049469	0.09715	0.0000976	0.91289	0.79745
11	0.04193	0.00023	3.882E-06	0.91311	0.79745
12	0.040798	5.729E-05	0.00241	0.91317	0.79986

Model 5					
Time period and Modal Participating Mass Ratios: After using NL links					
Mode	**Period**	**UX**	**UY**	**SumUX**	**SumUY**
1	0.191014	0.0000218	0.88802	0.0000218	0.88802
2	0.167929	0.55624	8.754E-05	0.55627	0.88811
3	0.094817	0.24511	1.425E-05	0.80137	0.88813
4	0.068678	6.703E-05	3.988E-05	0.80144	0.88817
5	0.067144	3.762E-05	8.346E-05	0.80148	0.88825
6	0.066621	1.978E-05	0.01232	0.8015	0.90057
7	0.064348	0.00304	0.00027	0.80454	0.90084
8	0.062097	1.266E-05	0.04785	0.80455	0.94869
9	0.058747	0.0821	2.114E-05	0.88665	0.94871
10	0.055682	0.00012	0.00027	0.88677	0.94898
11	0.054829	0.00345	3.783E-06	0.89022	0.94899
12	0.053538	0.00158	0.00014	0.8918	0.94913

C.2 Pushover results

The following pushover curves were obtained after performing pushover analysis in the building models considered.

#Model-1

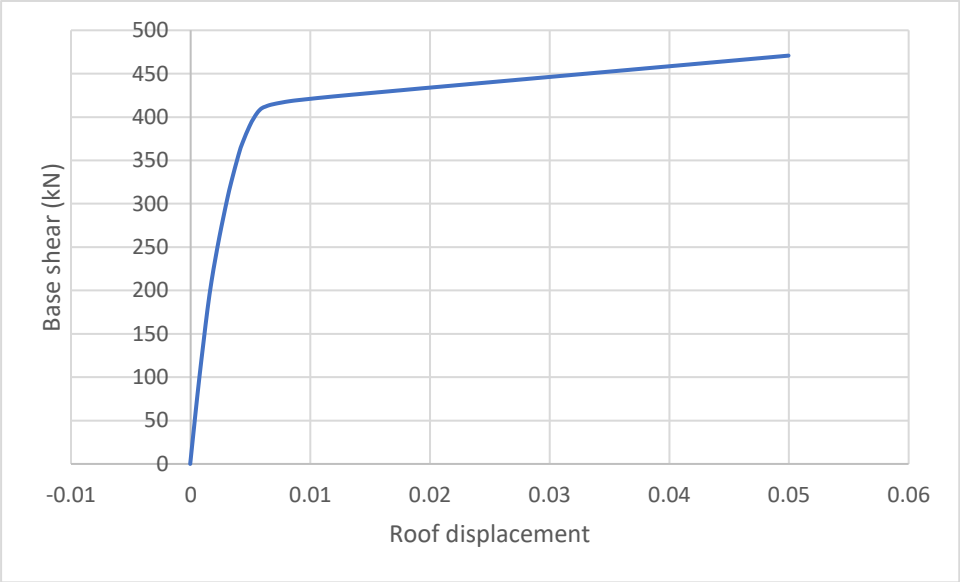

#Model-2

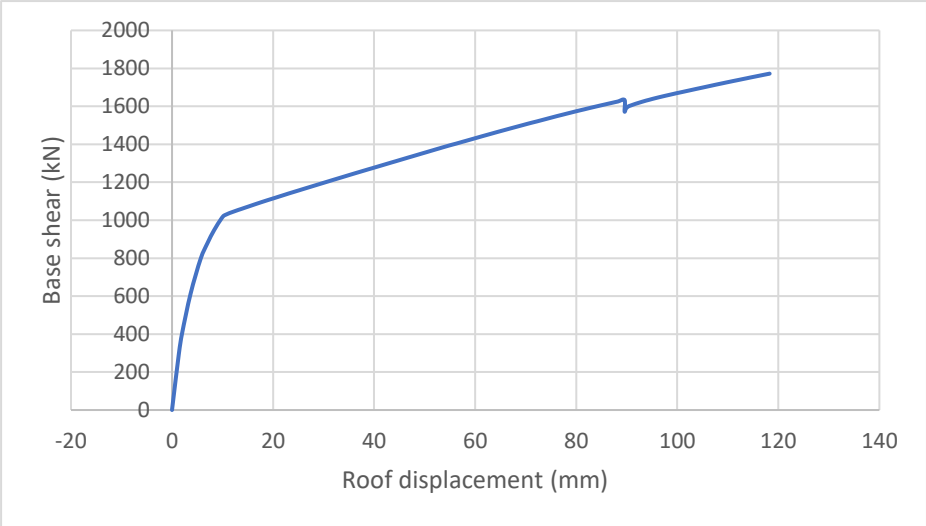

#Model-3

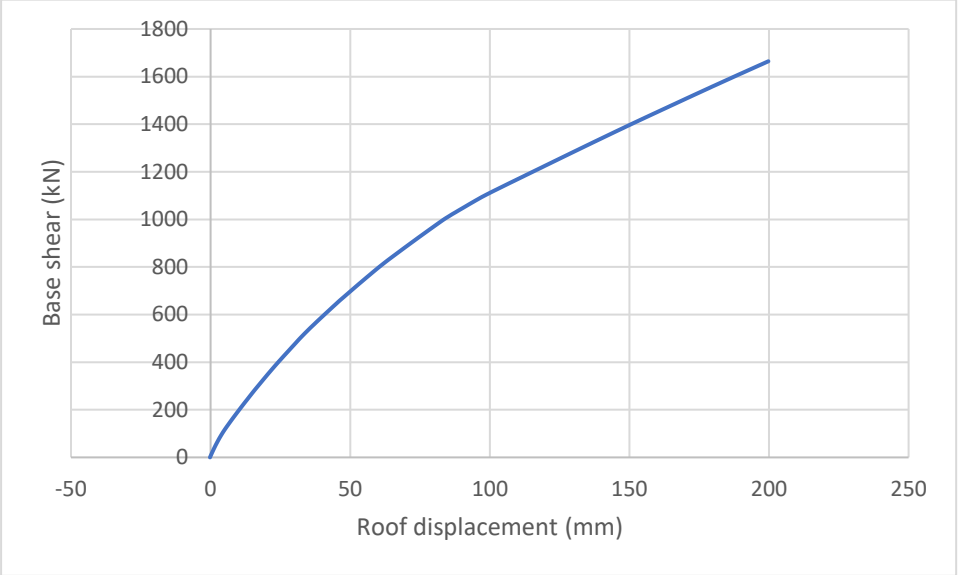

#Model-4

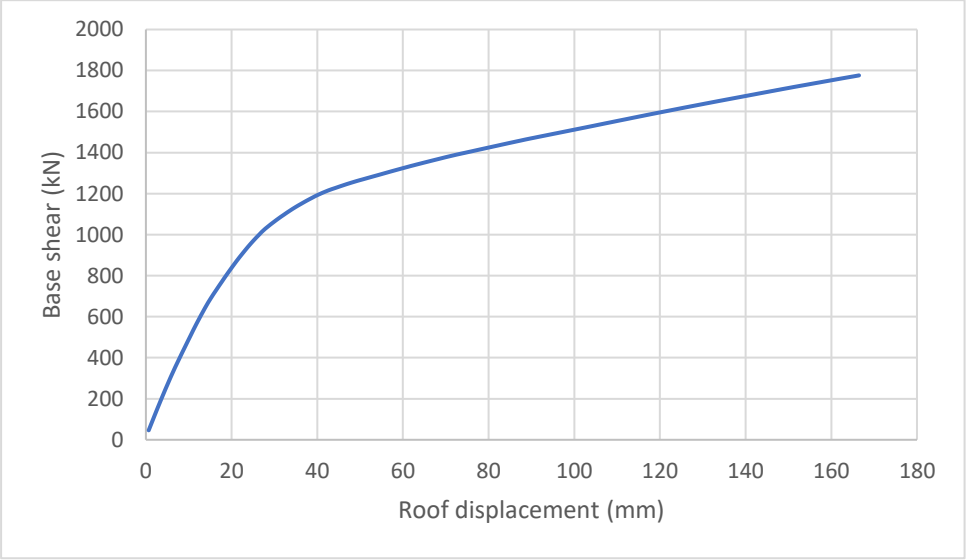

#Model-5

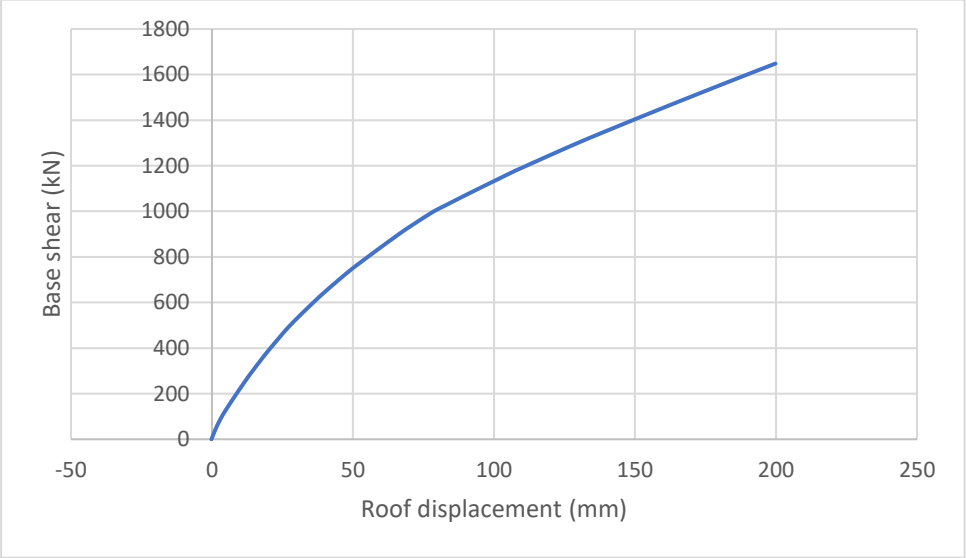

The following tables are obtained after pushover analysis for corresponding building models:

#Model 1

Step	Displacement (mm)	Base Shear (KN)
0	-0.000036	0
1	0.000297	44.068
2	0.000409	58.996
3	0.000743	101.411
4	0.001076	140.418
5	0.001409	178.418
6	0.001743	210.416
7	0.002076	237.427
8	0.002409	262.219
9	0.002743	284.972
10	0.003076	306.548
11	0.003409	325.899
12	0.004008	356.659
13	0.004341	370.554
14	0.00492	389.518
15	0.005253	398.133
16	0.005586	405.213
17	0.00592	409.913
18	0.006253	412.02
19	0.006586	413.72
20	0.00692	414.843
21	0.007253	415.813
22	0.007586	416.658
23	0.00792	417.503
24	0.008253	418.203
25	0.008586	418.852
26	0.00892	419.395
27	0.009253	419.891

Step	Displacement (mm)	Base Shear (KN)
28	0.009586	420.388
29	0.00992	420.885
30	0.010253	421.381
31	0.010586	421.878
32	0.01092	422.34
33	0.011253	422.803
34	0.011586	423.265
35	0.01192	423.727
36	0.012253	424.157
37	0.012586	424.586
38	0.01292	425.016
39	0.013253	425.445
40	0.013586	425.865
41	0.01392	426.285
42	0.014253	426.704
43	0.014586	427.124
44	0.01492	427.544
45	0.015253	427.964
46	0.015586	428.384
47	0.01592	428.803
48	0.016253	429.223
49	0.016586	429.643
50	0.01692	430.063
51	0.017253	430.483
52	0.017586	430.902
53	0.01792	431.322
54	0.018253	431.742
55	0.018586	432.162
56	0.01892	432.581
57	0.019253	433.001

Step	Displacement (mm)	Base Shear (KN)
58	0.019586	433.412
59	0.01992	433.822
60	0.020253	434.232
61	0.020586	434.643
62	0.02092	435.053
63	0.021253	435.464
64	0.021586	435.874
65	0.02192	436.284
66	0.022253	436.695
67	0.022586	437.105
68	0.02292	437.516
69	0.023253	437.926
70	0.023586	438.336
71	0.02392	438.747
72	0.024253	439.157
73	0.024586	439.568
74	0.02492	439.978
75	0.025253	440.388
76	0.025586	440.799
77	0.02592	441.209
78	0.026253	441.619
79	0.026586	442.03
80	0.02692	442.44
81	0.027253	442.85
82	0.027586	443.261
83	0.02792	443.671
84	0.028253	444.082
85	0.028586	444.492
86	0.02892	444.902
87	0.029253	445.313

Step	Displacement (mm)	Base Shear (KN)
88	0.029586	445.723
89	0.02992	446.133
90	0.030253	446.544
91	0.030586	446.954
92	0.03092	447.364
93	0.031253	447.775
94	0.031586	448.185
95	0.03192	448.596
96	0.032253	449.006
97	0.032586	449.416
98	0.03292	449.827
99	0.033253	450.237
100	0.033586	450.647
101	0.03392	451.058
102	0.034253	451.468
103	0.034586	451.878
104	0.03492	452.289
105	0.035253	452.699
106	0.035586	453.109
107	0.03592	453.52
108	0.036253	453.93
109	0.036586	454.34
110	0.03692	454.751
111	0.037253	455.161
112	0.037586	455.572
113	0.03792	455.982
114	0.038253	456.392
115	0.038586	456.803
116	0.03892	457.213
117	0.039253	457.623

Step	Displacement (mm)	Base Shear (KN)
118	0.039586	458.034
119	0.03992	458.444
120	0.040253	458.854
121	0.040586	459.265
122	0.04092	459.675
123	0.041253	460.085
124	0.041586	460.495
125	0.04192	460.906
126	0.042253	461.316
127	0.042586	461.726
128	0.04292	462.136
129	0.043253	462.547
130	0.043586	462.957
131	0.04392	463.367
132	0.044253	463.777
133	0.044586	464.187
134	0.04492	464.598
135	0.045253	465.008
136	0.045586	465.418
137	0.04592	465.828
138	0.046253	466.239
139	0.046586	466.649
140	0.04692	467.059
141	0.047253	467.469
142	0.047586	467.879
143	0.04792	468.29
144	0.048253	468.7
145	0.048586	469.11
146	0.04892	469.52
147	0.049253	469.93

Step	Displacement (mm)	Base Shear (KN)
148	0.049586	470.341
149	0.04992	470.751

Step	Displacement (mm)	Base Shear (KN)
150	0.049964	470.805

#Model 2

Step	Displacement (mm)	Base Shear (kN)
0	-0.002789	0
1	1.330545	291.899
2	1.997211	404.999
3	3.663878	611.927
4	5.663878	796.783
5	6.997211	878.211
6	8.330545	947.611
7	9.739512	1007.115
8	10.406179	1026.181
9	12.406179	1047.444
10	13.739512	1059.623
11	15.072846	1071.706
12	16.406179	1083.664
13	17.739512	1095.511
14	19.072846	1106.853
15	20.406179	1118.023
16	21.739512	1129.302
17	23.072846	1140.583
18	24.406179	1151.417
19	25.739512	1162.419
20	27.072846	1173.253
21	28.406179	1184.088
22	29.739512	1194.922
23	31.072846	1205.725
24	33.565513	1225.888
25	34.898846	1236.627
26	36.23218	1247.313
27	37.565513	1257.832
28	38.898846	1268.346
29	40.23218	1278.858
30	41.565513	1289.362
31	42.898846	1299.866
32	44.23218	1310.358
33	45.565513	1320.85
34	46.898846	1331.325
35	48.23218	1341.799
36	49.565513	1352.271
37	50.898846	1362.738
38	52.23218	1373.206
39	53.565513	1383.609
40	54.898846	1393.945
41	56.23218	1403.454
42	57.565513	1413.534
43	58.898846	1423.612
44	60.23218	1433.69
45	61.565513	1443.768
46	62.898846	1453.688
47	64.23218	1463.59
48	65.565513	1473.29

Step	Displacement (mm)	Base Shear (kN)
49	66.898846	1482.987
50	68.23218	1492.569
51	69.565513	1502.151
52	70.898846	1511.734
53	72.23218	1520.599
54	73.565513	1530.002
55	74.898846	1539.383
56	76.23218	1548.757
57	77.565513	1557.712
58	78.898846	1566.636
59	80.23218	1575.562
60	81.565513	1584.018
61	82.898846	1592.631
62	84.23218	1600.965
63	85.565513	1609.141
64	86.898846	1617.316
65	88.23218	1625.344
66	89.565513	1633.371
67	89.567513	1573.014
68	89.877693	1589.296
69	90.498054	1601.641
70	93.072108	1624.324
71	94.405441	1634.101
72	95.738775	1643.54
73	97.072108	1652.119
74	98.405441	1660.282
75	99.738775	1668.387
76	101.072108	1676.076
77	102.405441	1683.78
78	103.738775	1691.555

Step	Displacement (mm)	Base Shear (kN)
79	105.072108	1699.238
80	106.405441	1706.928
81	107.738775	1714.684
82	109.072108	1722.094
83	110.405441	1729.585
84	111.738775	1736.891
85	113.072108	1744.135
86	114.405441	1751.44
87	115.738775	1758.653
88	117.738775	1769.357
89	118.280441	1772.2

#Model 3

Step	Displacement (mm)	Base Shear (kN)
0	-0.219387	0
1	1.113947	34.702
2	2.44728	65.466
3	3.780613	93.198
4	5.113947	117.59
5	6.44728	139.848
6	7.780613	161.31
7	9.113947	182.335
8	10.44728	202.881
9	11.780613	223.304
10	13.113947	243.296
11	14.44728	263.229

Step	Displacement (mm)	Base Shear (kN)
12	15.780613	282.911
13	17.113947	301.795
14	18.44728	320.697
15	19.780613	339.463
16	21.113947	358.068
17	22.44728	376.213
18	23.780613	394.133
19	25.113947	411.621
20	26.44728	428.837
21	27.780613	445.932
22	29.113947	463.025
23	30.44728	480.117
24	31.780613	497.199
25	33.113947	513.509
26	34.44728	529.209
27	35.780613	544.728
28	37.113947	559.615
29	38.44728	574.446
30	39.780613	589.11
31	41.113947	603.642
32	42.44728	618.115
33	43.780613	632.491
34	45.113947	646.803
35	46.44728	660.972
36	47.780613	674.494
37	49.113947	688.036
38	50.44728	701.572
39	51.780613	715.108
40	53.113947	728.553

Step	Displacement (mm)	Base Shear (kN)
41	54.44728	741.783
42	55.780613	755.019
43	57.113947	768.161
44	58.44728	781.312
45	59.780613	794.309
46	61.113947	806.799
47	62.44728	819.138
48	63.780613	831.254
49	65.113947	842.904
50	66.44728	854.527
51	67.780613	866.139
52	69.113947	877.744
53	70.44728	889.337
54	71.780613	900.774
55	73.113947	912.212
56	74.44728	923.592
57	75.780613	934.917
58	77.113947	946.158
59	78.44728	957.408
60	79.780613	968.611
61	81.113947	979.755
62	82.44728	990.82
63	83.780613	1001.642
64	85.113947	1011.355
65	86.44728	1021.068
66	87.780613	1030.249
67	89.113947	1039.508
68	90.44728	1048.609
69	91.780613	1057.799

Step	Displacement (mm)	Base Shear (kN)
70	93.113947	1066.973
71	94.44728	1076.048
72	95.780613	1084.906
73	97.113947	1093.766
74	98.44728	1101.88
75	99.780613	1109.935
76	101.113947	1117.875
77	102.44728	1125.612
78	103.780613	1133.331
79	105.113947	1141.05
80	106.44728	1148.742
81	107.780613	1156.434
82	109.113947	1164.013
83	110.44728	1171.681
84	111.780613	1179.326
85	113.113947	1186.971
86	114.44728	1194.616
87	115.780613	1202.261
88	117.113947	1209.904
89	118.44728	1217.546
90	119.780613	1225.189
91	121.113947	1232.822
92	122.44728	1240.45
93	123.780613	1248.077
94	125.113947	1255.7
95	126.44728	1263.323
96	127.780613	1270.946
97	129.113947	1278.569
98	130.44728	1286.158

Step	Displacement (mm)	Base Shear (kN)
99	131.780613	1293.748
100	133.113947	1301.337
101	134.44728	1308.9
102	135.780613	1316.463
103	137.113947	1324.026
104	138.44728	1331.587
105	139.780613	1339.092
106	141.113947	1346.61
107	142.44728	1354.11
108	143.780613	1361.611
109	145.113947	1369.109
110	146.44728	1376.534
111	147.780613	1383.978
112	149.113947	1391.388
113	150.44728	1398.787
114	151.780613	1406.186
115	153.113947	1413.553
116	154.44728	1420.885
117	155.780613	1428.166
118	157.113947	1435.446
119	158.44728	1442.724
120	159.780613	1450
121	161.113947	1457.272
122	162.44728	1464.541
123	163.780613	1471.802
124	165.113947	1479.062
125	166.44728	1486.318
126	167.780613	1493.575
127	169.113947	1500.831

Step	Displacement (mm)	Base Shear (kN)
128	170.44728	1508.085
129	171.780613	1515.335
130	173.113947	1522.547
131	174.44728	1529.756
132	175.780613	1536.959
133	177.113947	1544.145
134	178.44728	1551.326
135	179.780613	1558.502
136	181.113947	1565.566
137	182.44728	1572.702
138	183.780613	1579.812
139	185.113947	1586.919
140	186.44728	1594.022
141	187.780613	1601.102
142	189.113947	1608.182
143	190.44728	1615.181
144	191.780613	1622.215
145	193.113947	1629.23
146	194.44728	1636.253
147	195.780613	1643.273
148	197.113947	1650.293
149	198.44728	1657.306
150	199.780613	1664.299

#Model 4

Step	Displacement (mm)	Base Shear (kN)
0	-0.020256	0
1	0.64641	46.058
2	2.096509	121.955
3	3.429843	190.232
4	5.763176	304.635
5	7.780134	395.144
6	9.113467	452.271
7	10.446801	508.806
8	11.780134	564.368
9	13.780134	641.877
10	15.113467	688.804
11	16.446801	731.086
12	17.780134	772.28
13	19.113467	812.496
14	21.113467	869.846
15	22.446801	905.335
16	23.780134	939.418
17	25.113467	971.06
18	26.446801	1000.272
19	27.863467	1028.891
20	30.46568	1071.501
21	32.233224	1097.456
22	33.566557	1116.376
23	34.89989	1134.035
24	36.233224	1150.245
25	37.566557	1165.989
26	38.89989	1180.703
27	40.233224	1194.775
28	42.566557	1215.492

Step	Displacement (mm)	Base Shear (kN)
29	44.233224	1227.596
30	46.844307	1246.121
31	49.214427	1261.297
32	50.54776	1269.158
33	51.881093	1276.938
34	53.214427	1284.71
35	54.845872	1294.268
36	56.301127	1302.84
37	57.63446	1310.657
38	59.130732	1319.189
39	61.130732	1330.555
40	62.464065	1337.928
41	63.797399	1345.1
42	65.901541	1356.224
43	67.234875	1363.226
44	68.568208	1370.186
45	69.901541	1377.114
46	71.234875	1383.786
47	72.568208	1390.258
48	73.901541	1396.378
49	75.234875	1402.474
50	76.568208	1408.675
51	77.901541	1414.876
52	79.234875	1421.007
53	80.568208	1427.145
54	81.901541	1433.284
55	83.234875	1439.422
56	84.568208	1445.538
57	85.901541	1451.588
58	87.234875	1457.598

Step	Displacement (mm)	Base Shear (kN)
59	88.568208	1463.592
60	89.901541	1469.338
61	91.234875	1474.947
62	92.568208	1480.556
63	93.901541	1486.157
64	95.234875	1491.741
65	96.568208	1497.294
66	97.901541	1502.879
67	99.234875	1508.474
68	100.568208	1514.073
69	101.901541	1519.663
70	103.234875	1525.251
71	104.568208	1530.936
72	105.901541	1536.624
73	107.234875	1542.291
74	108.568208	1547.944
75	109.901541	1553.589
76	111.234875	1559.231
77	112.568208	1564.859
78	113.901541	1570.494
79	115.234875	1576.101
80	116.568208	1581.683
81	117.901541	1587.267
82	119.234875	1592.786
83	120.568208	1598.24
84	121.901541	1603.69
85	123.234875	1609.139
86	124.568208	1614.585
87	125.901541	1620.031
88	127.234875	1625.4

Step	Displacement (mm)	Base Shear (kN)
89	128.568208	1630.786
90	129.901541	1636.108
91	131.234875	1641.446
92	132.568208	1646.749
93	133.901541	1652.049
94	135.234875	1657.259
95	136.568208	1662.478
96	137.901541	1667.697
97	139.234875	1672.915
98	140.568208	1678.135
99	141.901541	1683.353
100	143.234875	1688.572
101	144.568208	1693.791
102	145.901541	1698.988
103	147.234875	1704.184
104	148.568208	1709.374
105	149.901541	1714.528
106	151.234875	1719.684
107	152.734875	1725.288
108	154.068208	1730.27
109	156.380708	1738.908
110	157.714041	1743.888
111	159.047375	1748.869
112	161.047375	1756.329
113	162.380708	1761.299
114	163.802583	1766.49
115	165.135916	1771.352
116	166.46925	1776.213

#Model 5

Step	Displacement (mm)	Base Shear (kN)
1	-0.187443	0
2	1.145891	41.137
3	2.479224	76.347
4	3.812557	106.515
5	5.145891	132.985
6	6.479224	158.403
7	7.812557	183.342
8	9.145891	207.804
9	10.479224	231.655
10	11.812557	255.656
11	13.145891	278.991
12	14.479224	300.899
13	15.812557	322.83
14	17.145891	344.459
15	18.479224	365.729
16	19.812557	386.277
17	21.145891	406.206
18	22.479224	425.724
19	23.812557	445.242
20	25.145891	464.706
21	26.479224	483.317
22	27.812557	500.952
23	29.145891	518.158
24	30.479224	534.545
25	31.812557	550.83
26	33.145891	566.917
27	34.479224	582.823
28	35.812557	598.503
29	37.145891	614.091

Step	Displacement (mm)	Base Shear (kN)
30	38.479224	629.369
31	39.812557	644.157
32	41.145891	658.782
33	42.479224	673.22
34	43.812557	687.337
35	45.145891	701.418
36	46.479224	715.333
37	47.812557	729.072
38	49.145891	742.734
39	50.479224	755.615
40	51.812557	768.05
41	53.145891	780.476
42	54.479224	792.868
43	55.812557	805.23
44	57.145891	817.441
45	58.479224	829.69
46	59.812557	841.885
47	61.145891	853.939
48	62.479224	865.983
49	63.812557	877.878
50	65.145891	889.726
51	66.479224	901.574
52	67.812557	913.141
53	69.145891	924.308
54	70.479224	935.212
55	71.812557	945.934
56	73.145891	956.784
57	74.479224	967.589
58	75.812557	978.142
59	77.145891	988.348

Step	Displacement (mm)	Base Shear (kN)
60	78.479224	998.638
61	79.812557	1007.585
62	81.145891	1016.032
63	82.479224	1024.184
64	83.812557	1032.603
65	85.145891	1041.019
66	86.479224	1049.43
67	87.812557	1057.766
68	89.145891	1066.102
69	90.479224	1074.422
70	91.812557	1082.654
71	93.145891	1090.834
72	94.479224	1098.956
73	95.812557	1107.082
74	97.145891	1115.178
75	98.479224	1123.282
76	99.812557	1131.372
77	101.145891	1139.456
78	102.479224	1147.507
79	103.812557	1155.555
80	105.145891	1163.594
81	106.479224	1171.606
82	107.812557	1179.619
83	109.145891	1186.825
84	110.479224	1194.254
85	111.812557	1201.674
86	113.145891	1209.089
87	114.479224	1216.505
88	115.812557	1223.918
89	117.145891	1231.326

Step	Displacement (mm)	Base Shear (kN)
90	118.479224	1238.723
91	119.812557	1246.095
92	121.145891	1253.463
93	122.479224	1260.825
94	123.812557	1268.1
95	125.145891	1275.384
96	126.479224	1282.651
97	127.812557	1289.811
98	129.145891	1296.977
99	130.479224	1304.049
100	131.812557	1311.12
101	133.145891	1318.098
102	134.479224	1324.955
103	135.812557	1331.803
104	137.145891	1338.634
105	138.479224	1345.466
106	139.812557	1352.297
107	141.145891	1359.075
108	142.479224	1365.881
109	143.812557	1372.645
110	145.145891	1379.404
111	146.479224	1386.095
112	147.812557	1392.834
113	149.145891	1399.563
114	150.479224	1406.286
115	151.812557	1413.005
116	153.145891	1419.724
117	154.479224	1426.413
118	155.812557	1433.1
119	157.145891	1439.762

Step	Displacement (mm)	Base Shear (kN)
120	158.479224	1446.42
121	159.812557	1453.078
122	161.145891	1459.734
123	162.479224	1466.367
124	163.812557	1472.984
125	165.145891	1479.593
126	166.479224	1486.184
127	167.812557	1492.759
128	169.145891	1499.328
129	170.479224	1505.893
130	171.812557	1512.451
131	173.145891	1519.008
132	174.479224	1525.565
133	175.812557	1532.122
134	177.145891	1538.678
135	178.479224	1545.222
136	179.812557	1551.723
137	181.145891	1558.223
138	182.479224	1564.722
139	183.812557	1571.203
140	185.145891	1577.684
141	186.479224	1584.151
142	187.812557	1590.597
143	189.145891	1597.044
144	190.479224	1603.491
145	191.812557	1609.937
146	193.145891	1616.356
147	194.479224	1622.772
148	195.812557	1629.02
149	197.145891	1635.406

C.3 Performance points

The following curves are obtained for corresponding NBC 105 response spectrums for different PGA values:

#Model-1

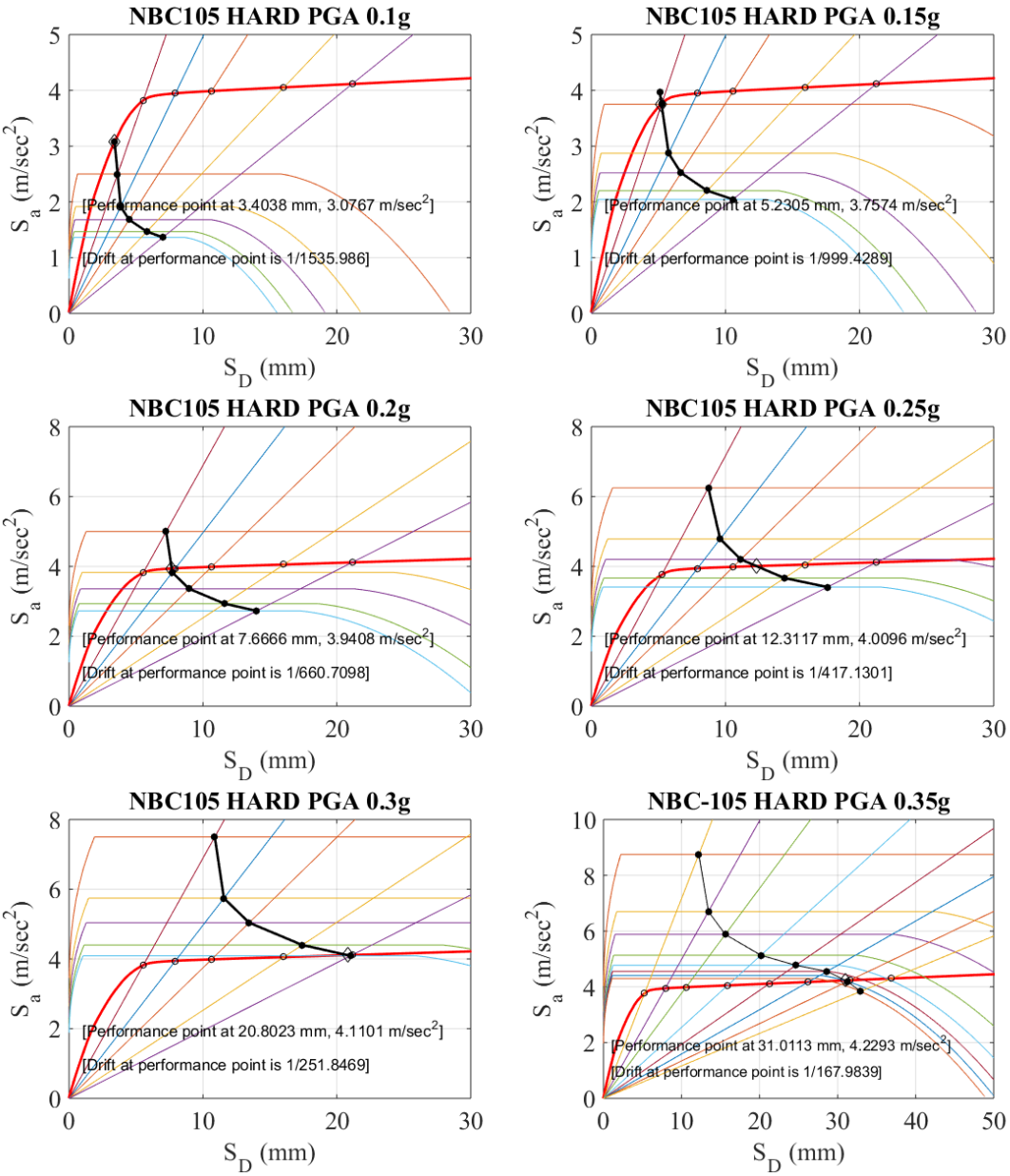

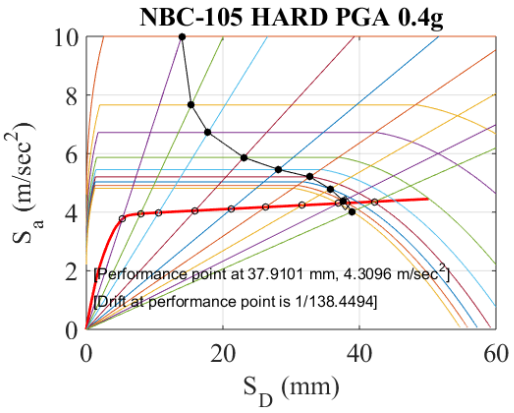
NBC-105 HARD PGA 0.4g
[Performance point at 37.9101 mm, 4.3096 m/sec^2]
[Drift at performance point is 1/138.4494]
S_a (m/sec^2)
S_D (mm)

#Model-3

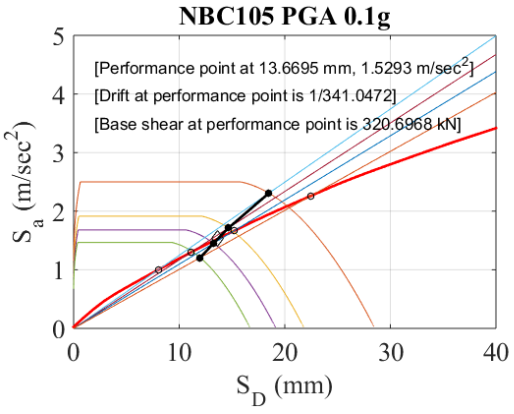
NBC105 PGA 0.1g
[Performance point at 13.6695 mm, 1.5293 m/sec^2]
[Drift at performance point is 1/341.0472]
[Base shear at performance point is 320.6968 kN]
S_a (m/sec^2)
S_D (mm)

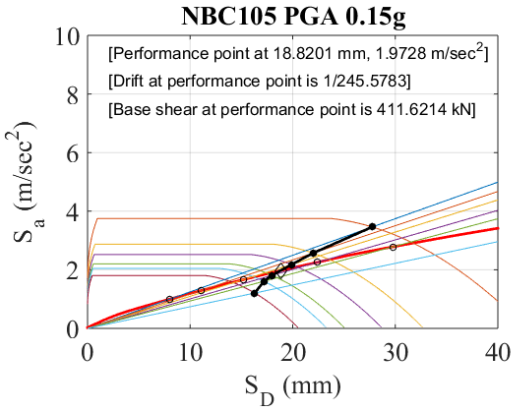
NBC105 PGA 0.15g
[Performance point at 18.8201 mm, 1.9728 m/sec^2]
[Drift at performance point is 1/245.5783]
[Base shear at performance point is 411.6214 kN]
S_a (m/sec^2)
S_D (mm)

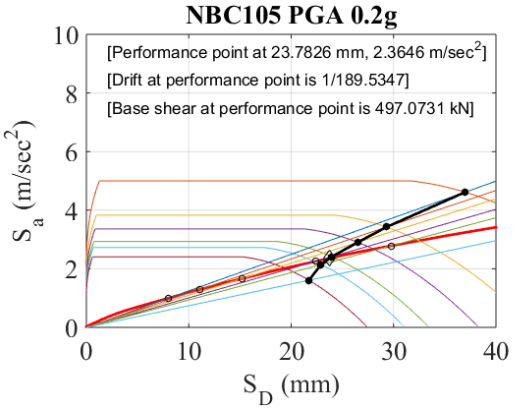
NBC105 PGA 0.2g
[Performance point at 23.7826 mm, 2.3646 m/sec^2]
[Drift at performance point is 1/189.5347]
[Base shear at performance point is 497.0731 kN]
S_a (m/sec^2)
S_D (mm)

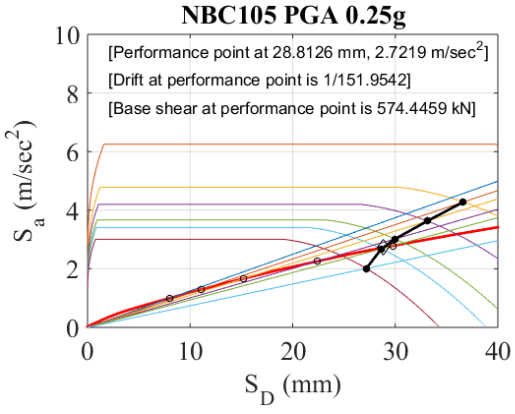
NBC105 PGA 0.25g
[Performance point at 28.8126 mm, 2.7219 m/sec^2]
[Drift at performance point is 1/151.9542]
[Base shear at performance point is 574.4459 kN]
S_a (m/sec^2)
S_D (mm)

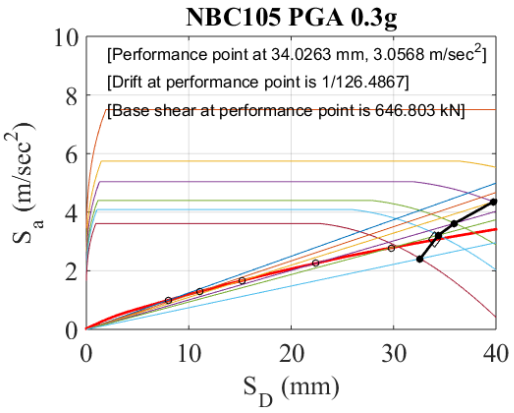
NBC105 PGA 0.3g
[Performance point at 34.0263 mm, 3.0568 m/sec^2]
[Drift at performance point is 1/126.4867]
[Base shear at performance point is 646.803 kN]
S_a (m/sec^2)
S_D (mm)

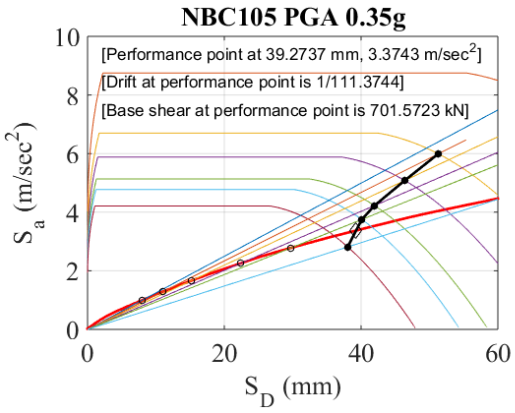
NBC105 PGA 0.35g
[Performance point at 39.2737 mm, 3.3743 m/sec^2]
[Drift at performance point is 1/111.3744]
[Base shear at performance point is 701.5723 kN]
S_a (m/sec^2)
S_D (mm)

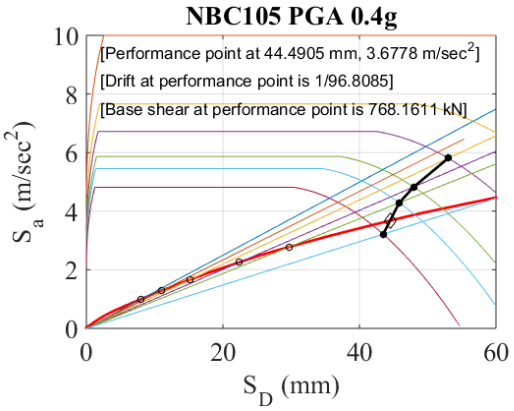
NBC105 PGA 0.4g
[Performance point at 44.4905 mm, 3.6778 m/sec^2]
[Drift at performance point is 1/96.8085]
[Base shear at performance point is 768.1611 kN]
S_a (m/sec^2)
S_D (mm)

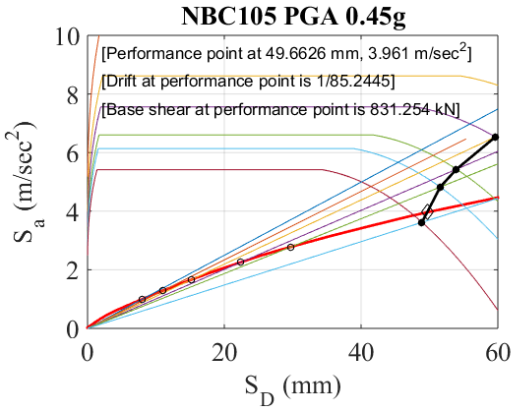
NBC105 PGA 0.45g
[Performance point at 49.6626 mm, 3.961 m/sec^2]
[Drift at performance point is 1/85.2445]
[Base shear at performance point is 831.254 kN]
S_a (m/sec^2)
S_D (mm)

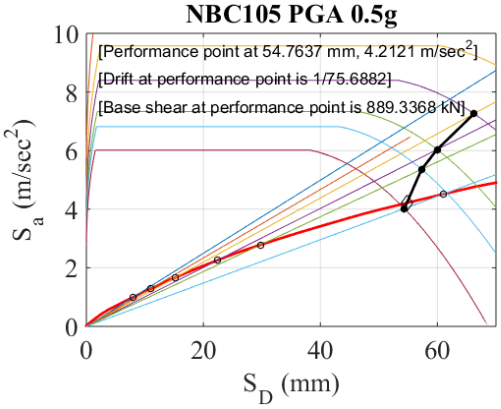
NBC105 PGA 0.5g
[Performance point at 54.7637 mm, 4.2121 m/sec^2]
[Drift at performance point is 1/75.6882]
[Base shear at performance point is 889.3368 kN]
S_a (m/sec^2)
S_D (mm)

#Model-4

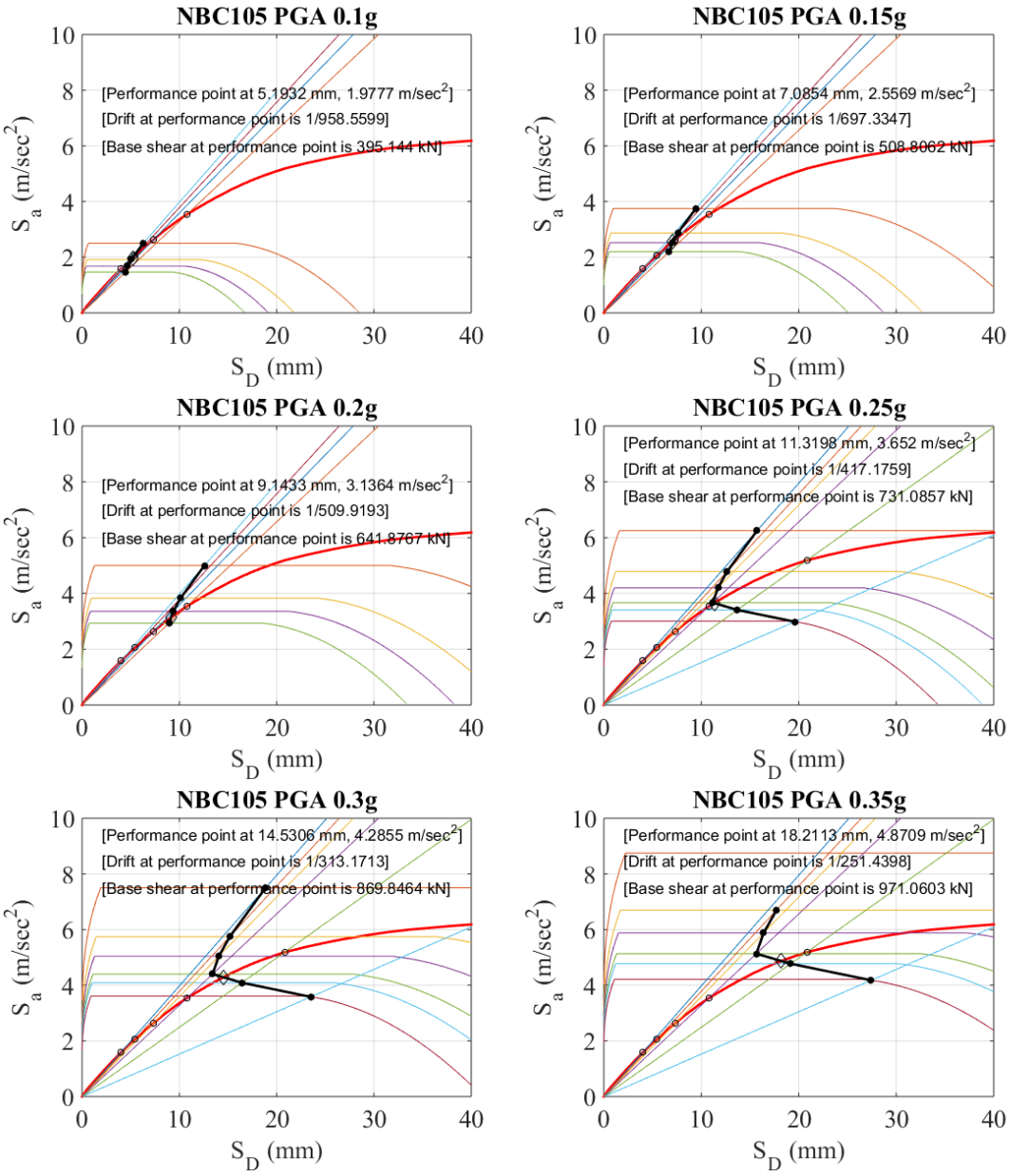
NBC105 PGA 0.1g
[Performance point at 5.1932 mm, 1.9777 m/sec^2]
[Drift at performance point is 1/958.5599]
[Base shear at performance point is 395.144 kN]
NBC105 PGA 0.15g
[Performance point at 7.0854 mm, 2.5569 m/sec^2]
[Drift at performance point is 1/697.3347]
[Base shear at performance point is 508.8062 kN]
NBC105 PGA 0.2g
[Performance point at 9.1433 mm, 3.1364 m/sec^2]
[Drift at performance point is 1/509.9193]
[Base shear at performance point is 641.8767 kN]
NBC105 PGA 0.25g
[Performance point at 11.3198 mm, 3.652 m/sec^2]
[Drift at performance point is 1/417.1759]
[Base shear at performance point is 731.0857 kN]
NBC105 PGA 0.3g
[Performance point at 14.5306 mm, 4.2855 m/sec^2]
[Drift at performance point is 1/313.1713]
[Base shear at performance point is 869.8464 kN]
NBC105 PGA 0.35g
[Performance point at 18.2113 mm, 4.8709 m/sec^2]
[Drift at performance point is 1/251.4398]
[Base shear at performance point is 971.0603 kN]
S_a (m/sec^2)
S_D (mm)

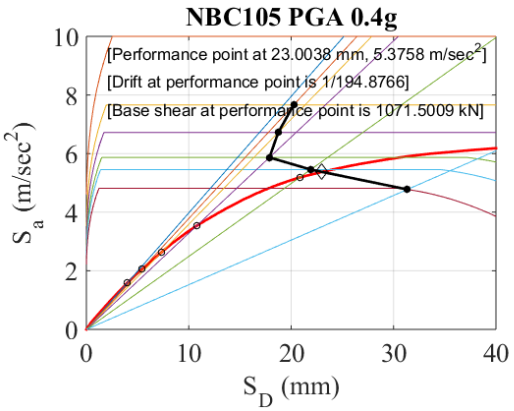
NBC105 PGA 0.4g
[Performance point at 23.0038 mm, 5.3758 m/sec^2]
[Drift at performance point is 1/194.8766]
[Base shear at performance point is 1071.5009 kN]
S_a (m/sec^2)
S_D (mm)

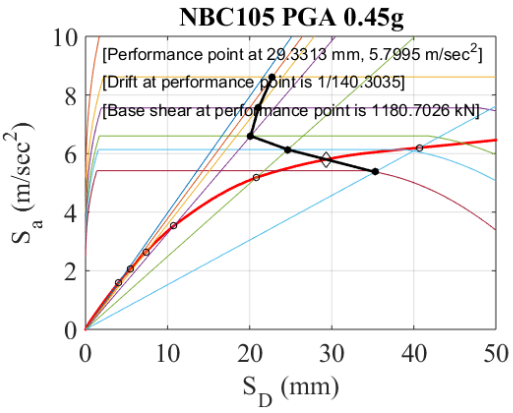
NBC105 PGA 0.45g
[Performance point at 29.3313 mm, 5.7995 m/sec^2]
[Drift at performance point is 1/140.3035]
[Base shear at performance point is 1180.7026 kN]
S_a (m/sec^2)
S_D (mm)

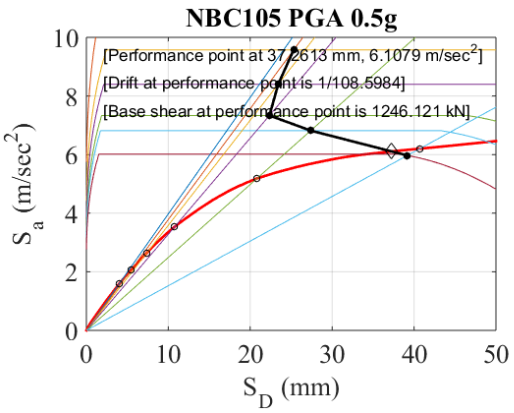
NBC105 PGA 0.5g
[Performance point at 37.2613 mm, 6.1079 m/sec^2]
[Drift at performance point is 1/108.5984]
[Base shear at performance point is 1246.121 kN]
S_a (m/sec^2)
S_D (mm)

#Model-5

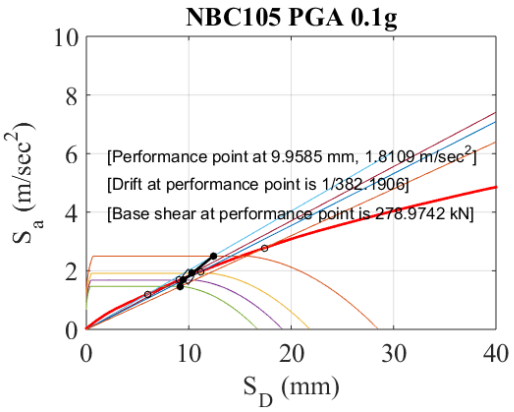
NBC105 PGA 0.1g
[Performance point at 9.9585 mm, 1.8109 m/sec^2]
[Drift at performance point is 1/382.1906]
[Base shear at performance point is 278.9742 kN]
S_a (m/sec^2)
S_D (mm)

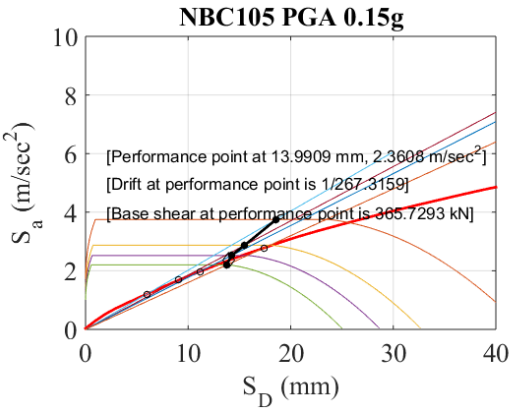
NBC105 PGA 0.15g
[Performance point at 13.9909 mm, 2.3608 m/sec^2]
[Drift at performance point is 1/267.3159]
[Base shear at performance point is 365.7293 kN]
S_a (m/sec^2)
S_D (mm)

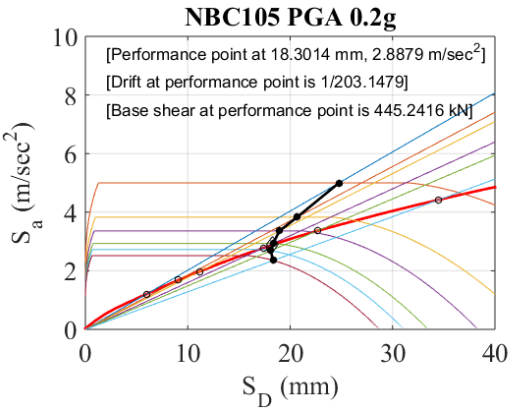
NBC105 PGA 0.2g
[Performance point at 18.3014 mm, 2.8879 m/sec^2]
[Drift at performance point is 1/203.1479]
[Base shear at performance point is 445.2416 kN]
S_a (m/sec^2)
S_D (mm)

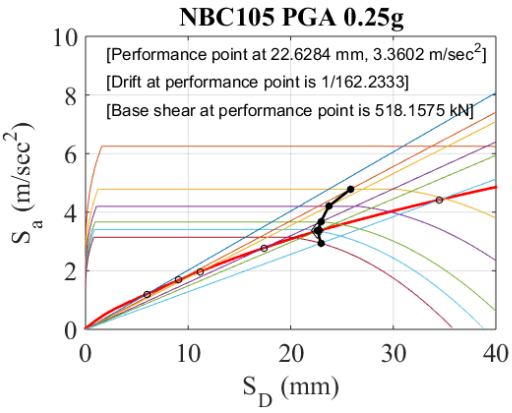
NBC105 PGA 0.25g
[Performance point at 22.6284 mm, 3.3602 m/sec^2]
[Drift at performance point is 1/162.2333]
[Base shear at performance point is 518.1575 kN]
S_a (m/sec^2)
S_D (mm)

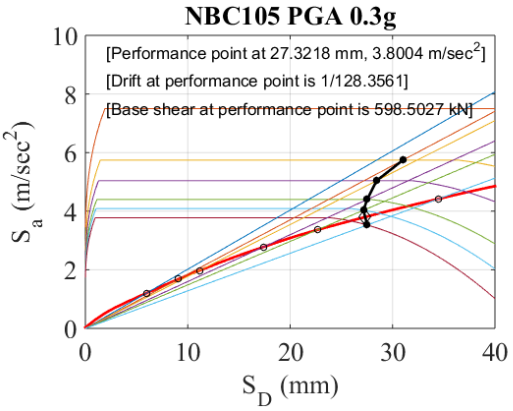
NBC105 PGA 0.3g
[Performance point at 27.3218 mm, 3.8004 m/sec^2]
[Drift at performance point is 1/128.3561]
[Base shear at performance point is 598.5027 kN]
S_a (m/sec^2)
S_D (mm)

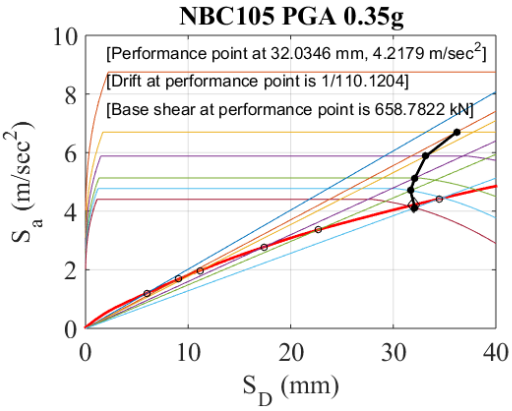
NBC105 PGA 0.35g
[Performance point at 32.0346 mm, 4.2179 m/sec^2]
[Drift at performance point is 1/110.1204]
[Base shear at performance point is 658.7822 kN]
S_a (m/sec^2)
S_D (mm)

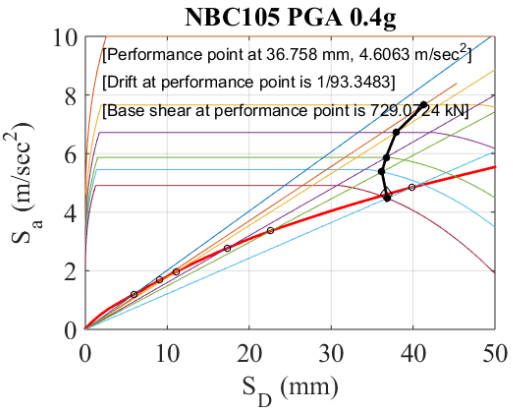
NBC105 PGA 0.4g
[Performance point at 36.758 mm, 4.6063 m/sec^2]
[Drift at performance point is 1/93.3483]
[Base shear at performance point is 729.0724 kN]
S_a (m/sec^2)
S_D (mm)

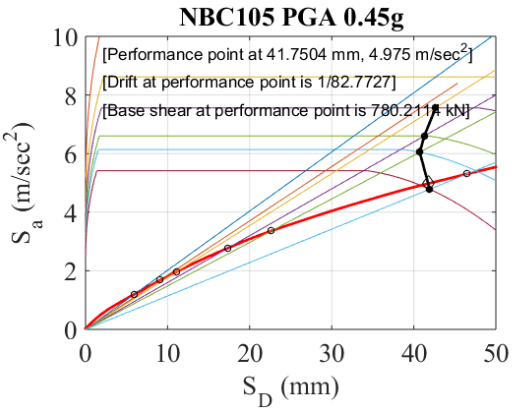
NBC105 PGA 0.45g
[Performance point at 41.7504 mm, 4.975 m/sec^2]
[Drift at performance point is 1/82.7727]
[Base shear at performance point is 780.2114 kN]
S_a (m/sec^2)
S_D (mm)

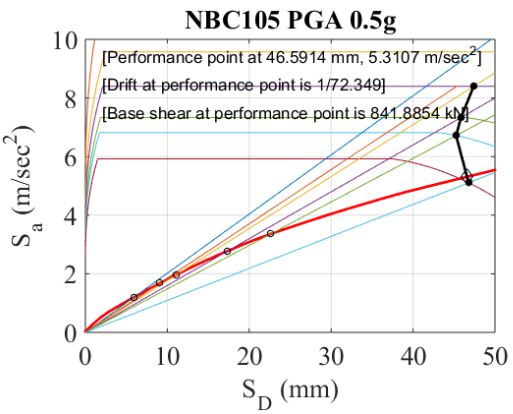
NBC105 PGA 0.5g
[Performance point at 46.5914 mm, 5.3107 m/sec^2]
[Drift at performance point is 1/72.349]
[Base shear at performance point is 841.8854 kN]
S_a (m/sec^2)
S_D (mm)